

AD-A123 035

DEVELOPMENT AND EVALUATION OF AN UNCOUPLED INCREMENTAL
CONSTITUTIVE MODEL..(U) TEXAS A AND M UNIV COLLEGE
STATION DEPT OF AEROSPACE ENGINEER..

1/1

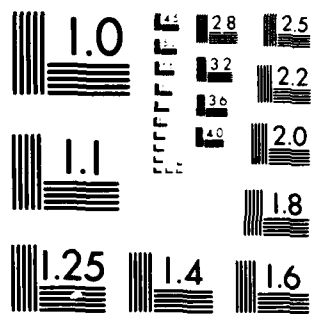
UNCLASSIFIED

J CRONENWORTH ET AL. MAY 82 TR-3275-82-1

F/G 20/11

NL

END
DATE
FILED
11-81
DTIC



MICROCOPY RESOLUTION TEST CHART
NATIONAL BUREAU OF STANDARDS-1963-A

AL A 123035



DEVELOPMENT AND EVALUATION OF AN UNCOUPLED,
INCREMENTAL CONSTITUTIVE MODEL FOR
ELASTIC-PLASTIC-CREEP BEHAVIOR AT ELEVATED TEMPERATURES



aerospace engineering department

TEXAS A&M UNIVERSITY

JEFF CRONENWORTH
AND
WALTER E. HAISLER

DTIC
ELECTE
JAN 4 1983
S D
H

OFFICE OF NAVAL RESEARCH
DEPARTMENT OF THE NAVY
WASHINGTON, D.C. 20025

CONTRACT #

TECHNICAL REPORT No. 3275-82-1

MAY 1982

DISTRIBUTION STATEMENT A
Approved for public release
Distribution Unlimited

DTIC FILE COPY

TEXAS A&M UNIVERSITY ENGINEERING EXPERIMENT STATION

067

Q

DEVELOPMENT AND EVALUATION OF AN UNCOUPLED,
INCREMENTAL CONSTITUTIVE MODEL FOR
ELASTIC-PLASTIC-CREEP BEHAVIOR AT ELEVATED TEMPERATURES

Jeff Cronenworth

and

Walter E. Haisler

Aerospace Engineering Department
Texas A&M University
College Station, Texas 77843

Office of Naval Research
Department of the Navy
Washington, D.C. 20025

Contract No. N00014-76-0150
Task No. NR 064-534

Technical Report No. 3275-82-1

May 1982

DTIC
SELECTED
JAN 4 1983
S H D

UNCLASSIFIED STATEMENT 1
Approved for public release
Distribution Unlimited

ABSTRACT

A uniaxial, uncoupled constitutive model for predicting the response of thermal and rate dependent elastic-plastic material behavior is presented. The model is based on an incremental classical plasticity theory extended to account for thermal, creep, and transient temperature conditions. Revisions to the combined hardening rule of the theory allow for better representation of cyclic phenomenon including the high rate of strain hardening upon cyclic reyield and cyclic saturation. Also, an alternative approach is taken to model the rate dependent inelastic deformation which involves hysteresis loops and stress relaxation tests at various temperatures. Evaluation of the model is performed by comparison with experiments involving various thermal and mechanical load histories on 5086 aluminum alloy, 304 stainless steel and Inconel X.

0-110
11-11-63

SECRETARY GENERAL
OFFICE OF THE SECRETARY
WASHINGTON, D.C.

Acknowledgements

This research was supported by the Office of Naval Research under Contract N00014-76-C-0150. The experimental results were obtained by Mr. Shik Yuen under the direction of Dr. Walter Bradley with the support of NASA Lewis Research Center through Grant NAG 3-31.

Accession For	
DTIC GRA&I	<input checked="" type="checkbox"/>
DTIC TAB	<input type="checkbox"/>
Unannounced	<input type="checkbox"/>
Justification	<input type="checkbox"/>
By _____	
Distribution/	
Availability Codes	
Dist	Avail and/or
	Special
A	



TABLE OF CONTENTS

	<u>Page</u>
ABSTRACT	ii
ACKNOWLEDGEMENTS	iii
TABLE OF CONTENTS.	iv
LIST OF FIGURES.	vi
CHAPTER I. INTRODUCTION	1
CHAPTER II. BACKGROUND.	4
Present Status of Constitutive Modeling	4
<u>Microphenomenological theories</u>	6
<u>Nonlinear viscoelastic theories.</u>	8
<u>Classical plasticity theories.</u>	8
Objectives.	10
CHAPTER III. DEVELOPMENT OF THE MODEL	11
Derivation of the Constitutive Equations.	11
Yield Function.	19
Hardening Rule.	20
Creep Strain Increment.	29
Experimental Data Requirements.	32
Construction of Yield Surface Size and Stress vs. Equivalent Uniaxial Plastic Strain Diagrams.	37
Computational Considerations.	38
<u>Gradients.</u>	40
<u>Transition step.</u>	40
<u>Thermal and elastic strain increments.</u>	41
Extension to Multiaxial Theory.	42

	<u>Page</u>
CHAPTER IV. EVALUATION OF THE MODEL	43
Theoretical Model Capabilities.	43
<u>Example 1 - Change of strain hardening with stress reversal</u>	43
<u>Example 2 - Cyclic saturation.</u>	45
<u>Example 3 - Cyclic thermomechanical loading.</u>	49
Comparison with Experiment.	52
<u>Cyclic thermomechanical load test on 5086 aluminum alloy</u>	53
<u>Cyclic loading of 304 stainless steel at 1000°F</u>	53
<u>Cyclic saturation of Hastelloy-X</u>	57
CHAPTER V. CONCLUSIONS.	69
REFERENCES	71
APPENDIX. COMPUTER PROGRAM OUTLINE.	74

LIST OF FIGURES

FIGURE		Page
1	Total strain decomposition	13
2	Plasticity models	21
3	Definition of standard hardening rules	25
4	Typical experimental results showing difference in first and second quarter cycle response	27
5	Mechanical response of typical ductile metal exhibiting cyclic saturation in cyclic loading . .	28
6	Experimental characterization of the rate dependence of the model	30
7	Uniaxial isothermal single cycle reverse loading curves and their linear representations input to the model	33
8	Hardening ratio	35
9	Construction and evolution of K vs. $\frac{-P}{\epsilon}$ diagrams	39
10	Change of strain hardening with stress reversal . .	44
11	Hardening rules used in Example 2	46
12	Modeling of cyclic saturation using kinematic and isotropic hardening laws	47
13	Modeling of cyclic saturation using combined hardening law	48
14	Input for Example 3	50
15	Cyclic thermomechanical loading	51
16	Comparison of Allen and Haisler model to experiment for aluminum cyclic load test	54
17	Comparison of revised model to experiment for aluminum cyclic load test	55

LIST OF FIGURES (continued)

FIGURE		Page
18	Comparison of model and experiment for 304 stainless steel at 1000°F using first cycle data as input . . .	56
19	Comparison of model and experiment for 304 stainless steel at 1000°F using fourth cycle data as input	58
20	Experimental hysteresis loops for hastelloy-X at room temperature	60
21	Experimental hysteresis loops for hastelloy-X at 500°F	61
22	Experimental hysteresis loops for hastelloy-X at 900°F	62
23	Experimental hysteresis loops for hastelloy-X at 1200°F	63
24	Experimental hysteresis loops for hastelloy-X at 1400°F	64
25	Experimental hysteresis loops for hastelloy-X at 1600°F	65
26	Cyclic saturation of hastelloy-X at room temperature	67

CHAPTER I

INTRODUCTION

Modern computational methods for the stress analysis of structures are well established. For behavior that is linear and even geometrically nonlinear, the finite element method has proven to be a very capable tool for the structural engineer. However, nonlinear material analysis is much more difficult and not yet as fully developed as proven by the large amount of research done in this area in recent years. Of particular interest to this research, the solution of thermal and rate dependent elastic-plastic material behavior is quite difficult. Applications of this technology are needed in components such as nuclear reactor pressure vessels and gas turbine blades.

Historically, the study of plasticity of metals began in 1864 with the publishing by Tresca [1] of a preliminary account of experiments on punching and extrusion. This led him to state that a metal yielded plastically when the maximum shear stress attained a critical value. Application of Tresca's yield criterion was investigated by Saint-Venant [2] to determine stresses in cylinders and tubes. He also recognized that there was not a one-to-one relation between stress and total plastic strain. Levy in 1871 proposed multiaxial relations between stress and plastic strain [2].

Advancement to a more satisfactory yield criterion was constructed on the basis of purely mathematical considerations by von Mises [3]

This thesis follows the style and format of the Journal of Applied Mechanics.

in 1913. Further work was done in the 1920's by Prandtl [4], Nadai, Lode, and von Karman [2]. It was in the early 1930's that two important generalizations of the available theory were made. The first was made by Reuss in 1930 [5] who allowed for the elastic component of strain. The second was made by Schmidt (1932) and Odquist (1933) [2] who showed how to incorporate work hardening into the framework of the Levy-Mises equations. Thus by 1932 an elastic-plastic theory had been constructed to model these properties of an isotropic metal at room temperature [2].

Work in this area in the 1940's and beyond was done by several prominent researchers like Hill [2], Drucker [6], Prager [7], and Ziegler [8]. Recently, the basic trend has been to extend the rate independent theories to include rate effects by adding on a creep term. This leads to an uncoupled or partitioned theory, and many are now in use today in finite element structural analysis codes. Most recently with the recognition that the rate independent and rate dependent inelastic deformations are not autonomous phenomenon, a number of "unified" constitutive models have been developed and are still undergoing active development [9]. Present day efforts include the extension of classical plasticity to predict rate dependent behavior and the modification of linear viscoelasticity to model nonlinear material response [10]. Many theories are available but none have shown clear superiority over the others in modelling material behavior over wide ranges of temperature and load.

→The purpose of this research is to extend the classical incremental theory of plasticity to develop and evaluate the uniaxial

constitutive relations necessary to model the nonlinear behavior of crystalline materials experiencing thermoelastic-plastic-creep. Among the requirements for a sound constitutive theory for the media mentioned above are that it incorporate the ability to model transient temperature response; cyclic behavior including cyclic saturation, the change in strain hardening upon stress reversal, and the Bauschinger effect; and rate dependence.

In fulfillment of these objectives, this thesis will proceed in the following manner. First, a brief literature review of the available theories is presented along with a discussion of the details of the constitutive model used in this research. Next, the development of the model is accomplished by derivation of the uniaxial theory including experimental data requirements and computational considerations. Several theoretical examples are presented along with comparison to experiments on several different metals at elevated temperature.

CHAPTER II

BACKGROUND

Present Status of Constitutive Modelling

To characterize the structural response of any general three-dimensional body, one must satisfy mechanics (conservation of mass and momentum, and kinematics), thermodynamics, and constitution. Since mechanics and thermodynamics are well established for most continua, it becomes the physical characteristics or constitution of a body that determines whether one can successfully analyze its structural response. Furthermore, because of the widely varying material properties and environments that structural media are subjected to, constitutive modelling is usually restricted to specific types of media. An all encompassing model that works equally well for all materials is simply not feasible. One such category of material response, and the one that this research will deal specifically with, is the elastic-plastic-rate-dependent crystalline material at elevated temperature.

The major types of constitutive laws available to model the material behavior discussed above can be grouped into three categories, microphenomenological, nonlinear viscoelastic, and classical plasticity. Also, there is an existing subdivision within the categories labeled unified and uncoupled theories, where the two differ in their approach to the treatment of rate independent and rate dependent inelastic deformation. The unified approach separates the total strain as

$$\epsilon = \epsilon^E + \epsilon^I + \epsilon^T, \quad (1)$$

where ϵ represents the total strain and superscripts E, I, and T represent the elastic, inelastic, and thermal components respectively. Alternatively, the uncoupled theories partition the inelastic strain into plastic and creep components. This can be expressed as

$$\epsilon = \epsilon^E + \epsilon^P + \epsilon^C + \epsilon^T, \quad (2)$$

where superscripts P and C represent the rate independent "plasticity" and rate dependent "creep" strain terms respectively. Researchers like Walker [9] and Krieg [11] question the partitioning as it has no underlying physical basis and does not account for creep and plasticity interaction.

The uncoupling of inelastic behavior into rate independent and rate dependent components is unsatisfactory to the material scientist because it is not microphysically justified [11]. Although many recent unified theories have been proposed, they still are not yet proven to be more successful overall than the uncoupled theories.

For example, Walker's theory [9] (considered one of the better unified models) reproduces cyclic stress-strain behavior at elevated temperatures very well. Unfortunately, the theoretical hysteresis loops at smaller strain rates or lower temperatures are too square in comparison with the actual experimental loops. Thus, Walker's theory does not characterize adequately the classical plasticity that is occurring in this load-temperature range. Walker also proposes an extension to include temperature dependence, but no attempt has been made to model transient temperature response [10]. His theory is restricted in its

use to an elevated temperature environment. The author does not want to leave the impression that Walker's theory is an inferior one as it is not. This discussion is simply to point out that the uncoupled theories are not necessarily inferior to the unified ones.

As discussed below, present theories attempt to model these physical mechanisms in a variety of ways.

Microphenomenological theories. The mechanisms for microphenomenological theories are discussed in detail by Allen [12]. These theories represent an element of material called a polycrystal as being composed of a large number of randomly oriented monocrystals. Statistical averages of the properties of each monocrystal and their interactions determine the behavior of the polycrystal [13]. These crystalline materials form lattice structures that contain many imperfections called dislocations which vary in density and location depending upon the processing used in manufacturing the material. Plastic deformation occurs by slip on certain crystallographic planes and is explained in terms of dislocation theory of plastic deformation. For example, dislocation interaction explains how strain hardening can occur in any crystal [14].

One example of a microphysically based constitutive law is an elastic-viscoplastic theory based on two internal state variables by Bodner, et al. [15]. The authors state the constitutive equations ability to represent the principal features of cyclic loading behavior including softening upon stress reversal, cyclic hardening or softening, cyclic saturation, cyclic relaxation, and cyclic creep. One limitation of the formulation though is that the computed stress-strain

curves are independent of the strain amplitude and therefore too "flat" or "square".

Another example is in the paper by Miller [16] on modelling of cyclic plasticity with unified constitutive equations. He also recognizes the shortcoming of many theories in predicting hysteresis loops which are "oversquare" in comparison to observed experimental behavior. Improvement is accomplished by making the kinematic work-hardening coefficient depend on the back stress and the sign of the nonelastic strain term. Results compare favorably with that observed in 2024-T4 aluminum alloy. Miller states his approach appears consistent with an existing physical explanation in terms of annihilation of previously-generated dislocation loops upon reversals in the direction of dislocation motion.

A theory that is similar in format to Miller's is by Krieg, Swearingen, and Rohde [11]. The model uses two internal state variables to reflect current microstructure and is based upon models for dislocation process in pure metals. It is an extension of an equation of state theory originally attributed to Kocks [17] where the inelastic flow rule is taken to be a power function incorporating a kinematic and isotropic internal variable. They assume that all the net mechanical effect of the complex dislocation processes can be contained by one or two readily measurable macroscopic variables. The theory cannot accurately model cyclic hardening or softening behavior and the strain hardening behavior is necessarily "square" in nature because of the power law assumption. Also, applications of the model over a wide range of homologous temperatures, or to alloys in general is not advised.

Nonlinear viscoelastic theories. Nonlinear viscoelastic or thermodynamically based theories are usually distinguished by their single integral or convoluted form. This type of constitutive model employs the first and second laws of thermodynamics along with physical constraints to complete the formulation [12]. A detailed review of several existing theories is presented in both [10] and [18].

One of the more promising theories is credited to Walker [9,18]. It is a unified integral viscoplastic theory developed by modifying the constitutive relation for a linear three parameter viscoelastic solid. The theory contains clearly defined material parameters, a rate dependent equilibrium stress, and a proposed multiaxial model. An important shortcoming of Walker's theory is its failure to model transient temperature conditions, but Allen and Milly [10] conclude that his theory is the best presently available for predicting cyclic response at elevated temperatures under isothermal conditions.

Other nonlinear viscoelastic theories discussed by Walker [18] are by Cernochy and Krempl, Valanis, and Chaboche.

Classical plasticity theories. The type of constitutive law considered in this research is derived from classical incremental plasticity. It is termed a macrophenomenological theory as it derives its state variables purely from experimental results without direct reference to the microstructure of the material. This type of constitutive law can be defined as one that attempts to describe the elastic-plastic behavior of a material based on properties obtained from a single stress state and then use them to establish relationships between the general stress and strain tensors [13]. Most incremental

plasticity theories have four major components: (1) a stress-elastic strain relation, (2) a yield function describing the onset of plastic deformation, (3) a hardening rule which prescribes the strain-hardening of the material and the modification of the yield surface during plastic flow, and (4) a flow rule which defines the component of strain that is plastic or nonrecoverable [19].

Research in this area is voluminous. The inviscid plasticity is well established while the extension to include rate and thermal effects is not. References [10,12] and [13] summarize some of the important research efforts in their field of study. Of the classical plasticity theories reviewed in [10], the most promising ones belong to Zienkiewicz and Corneau, and Allen and Haisler. The former is a rate dependent unified theory which allows for nonassociative plasticity and strain softening but does not model the Bauschinger effect or temperature dependence. The latter is an extension of classical plasticity to model both rate and thermal effects. It is a two state variable uncoupled theory with clearly defined material parameters and extension to multiaxial form. Still another example is a model proposed by Popov and Petersson [20,21]. Excellent agreement with experiment is shown in the isothermal, rate independent case. Snyder and Bathe [22] have proposed a modification to classical plasticity which does model both rate and thermal effects in the monotonic load case but is restricted to a kinematic hardening rule. Allen [12] suggests that the theory proposed by Yamada and Sakurai [23,24] may be the best for modelling the type of behavior described herein. Temperature dependence of material properties, a combined hardening rule, and an

uncoupled rate dependent creep term are all included in the formulation, but the mathematical consistency of the theory is questioned [12].

The one classical incremental plasticity theory surveyed that has all the necessary components to model the thermoelastic-plastic-creep material behavior is the one presented by Allen and Haisler [25]. Rate and thermal effects, the Bauschinger effect, a combined hardening rule as well as an extension to multiaxial loadings are all included in their formulation.

Objectives

The objective of this research is to model thermoelastic-plastic creep behavior of metals at elevated temperatures using the theory presented by Allen and Haisler with the addition of a revised hardening rule. Their theory is an uncoupled, incremental, nonisothermal constitutive model based on the classical theory of plasticity for the analysis of crystalline materials. Special emphasis is placed on modelling of cyclic thermomechanical load histories which includes transient temperature response, the Bauschinger effect, cyclic saturation, different degrees of strain hardening, and rate effects. Evaluation of the uniaxial theory is performed by comparison with experiment.

CHAPTER III

DEVELOPMENT OF THE MODEL

The author gives the following justifications for using the uncoupled approach proposed by Allen and Haisler. One can partition the total inelastic strain into components as long as their sum yields the total nonrecoverable deformation without significant adverse effects [12]. The theory is able to model behavior over a wide range of load and temperature up to at least one-half the melting point for several metals. It is also one of only a few to address transient temperature conditions. Also, with the revised hardening law presented herein, the rate independent inelastic deformation is modeled as well as or better than the unified theories reviewed. Reasonable experimental data requirements are another strong point of this theory.

Derivation of the Constitutive Equations

The constitutive equations of the Allen and Haisler model are derived in a uniaxial incremental form relating the total stress increment to the total strain increment. Development of the theory in this form is a logical approach as it lends itself to much simpler evaluation without introducing unnecessary complications of a multiaxial theory. Many components of the work required are much more easily done in uniaxial form such as the computer code development and experimental model verification.

As stated earlier, most classical plasticity theories have four major components. First, there is a relation between stress and elastic strain

$$\sigma = E\epsilon^E = E(\epsilon - \epsilon^P - \epsilon^C - \epsilon^T), \quad (3)$$

or in incremental form

$$\Delta\sigma = E^{t+\Delta t} (\Delta\epsilon - \Delta\epsilon^P - \Delta\epsilon^C - \Delta\epsilon^T) + \Delta E (\epsilon^t - \epsilon^P{}^t - \epsilon^C{}^t - \epsilon^T{}^t) \quad (4)$$

where σ is the uniaxial stress, E is the elastic modulus, and ϵ is the uniaxial strain. Superscripts P, C, and T denote plastic, creep, and thermal components respectively while t denotes values at the start of the load step, and $t + \Delta t$ denotes values at the end of a load step. Note that the elastic modulus is measured at the end of the step because the time step is finite rather than infinitesimal as described by Allen [12]. A graphical decomposition of the total strain is shown in Fig. 1. The term "zero time" denotes a loading input short enough to negate any time dependent deformation but long enough to disregard inertial effects (a few seconds for many metals) [12]. Conversely, the long time curve characterizes the rate dependent deformation. Recall that there is no physical basis for uncoupling the inelastic deformation, but it is valid as long as coupling effects are insignificant or the uncoupling is done properly.

Secondly, a yield function describes the onset of plastic deformation. A possible functional form, supported by experiment, is given by

$$F(\sigma - \alpha) = K^2 (\int d\epsilon^{\bar{P}}, T) \quad (5)$$

where α and K represent the center and radius of the yield surface respectively, $\int d\epsilon^{\bar{P}}$ is the history of the equivalent uniaxial plastic

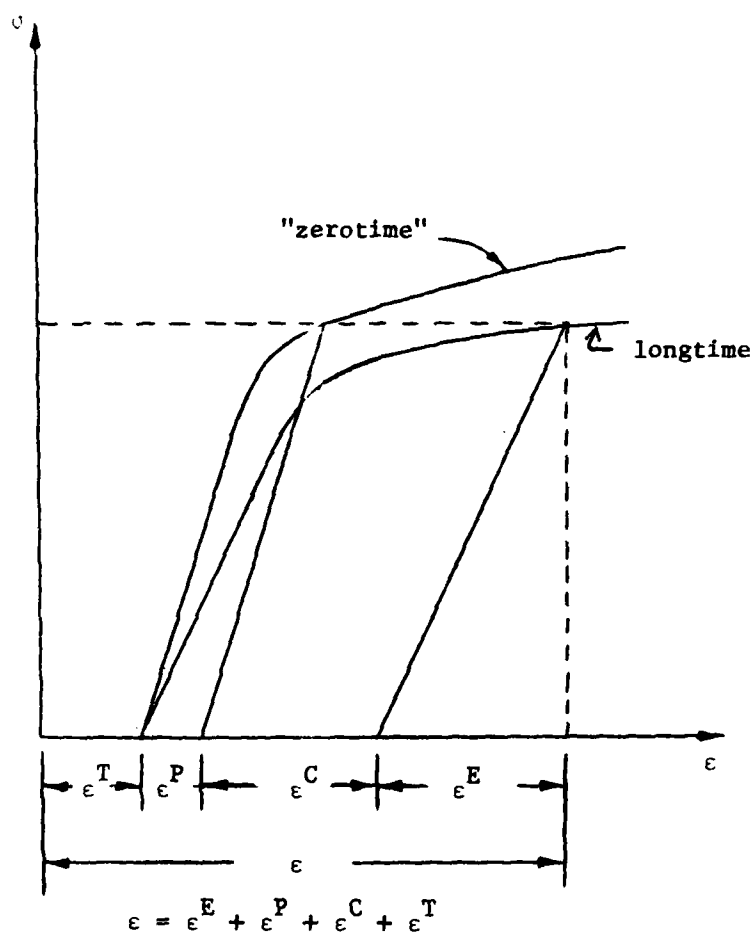


Fig. 1 Total strain decomposition

strain and T is the temperature. Note that microphysically α is a state variable combining the effects of the back and drag stresses while $d\epsilon^{-P}$ is a second state variable representing the dislocation arrangement. This arrangement of dislocations and dislocation loops will be discussed later as to their effect on reyield and strain hardening behavior upon reyield.

A hardening rule prescribes the strain hardening of the material and the modification of the yield surface during plastic flow and can be stated in a combined isotropic-kinematic form as

$$d\alpha = d\mu(\sigma - \alpha) \quad (6)$$

where $d\mu$ is a scalar. Lastly, if yielding does occur we need further information concerning the rate of deformation to complete the description of the material behavior. This information is provided by the flow rule which defines the component of strain that is plastic or nonrecoverable and can be written as

$$d\epsilon^P = d\lambda \frac{\partial F}{\partial \sigma} \quad (7)$$

where $d\lambda$ is a scalar determined from material data. Equation (7) is called an associated flow rule because it is the less general case containing the partial derivative of the yield function rather than a general plastic potential. It is also known as a normality condition because it can be interpreted as requiring the normality of the plastic strain increment "vector" to the yield surface in n stress dimensions [26].

Differentiation of (5) is the first step in deriving the constitutive equations and will yield

$$\frac{\partial F}{\partial \sigma} d\sigma - \frac{\partial F}{\partial \alpha} d\alpha = 2K \frac{\partial K}{\partial \bar{\epsilon}^P} d\bar{\epsilon}^P + 2K \frac{\partial K}{\partial T} dT. \quad (8)$$

The above consistency condition requires that loading from a plastic state must lead to another plastic state [27]. Substitution of (7) into (4)

$$d\sigma = E^{t+\Delta t} (d\epsilon - d\lambda \frac{\partial F}{\partial \sigma} - d\epsilon^C - d\epsilon^T) + dE(\epsilon^t - \epsilon^P - \epsilon^C - \epsilon^T) \quad (9)$$

and then (9) into (8) yields

$$\begin{aligned} \frac{\partial F}{\partial \sigma} \{E^{t+\Delta t} (d\epsilon - d\lambda \frac{\partial F}{\partial \sigma} - d\epsilon^C - d\epsilon^T) + dE(\epsilon^t - \epsilon^P - \epsilon^C - \epsilon^T)\} \\ - \frac{\partial F}{\partial \alpha} d\alpha = 2K \frac{\partial K}{\partial \bar{\epsilon}^P} d\bar{\epsilon}^P + 2K \frac{\partial K}{\partial T} dT. \end{aligned} \quad (10)$$

Solving for $d\lambda$ from above

$$\begin{aligned} d\lambda = \{ \frac{\partial F}{\partial \sigma} [E^{t+\Delta t} (d\epsilon - d\epsilon^C - d\epsilon^T) + dE(\epsilon^t - \epsilon^P - \epsilon^C - \epsilon^T)] - \frac{\partial F}{\partial \alpha} d\alpha \\ - 2K \frac{\partial K}{\partial \bar{\epsilon}^P} d\bar{\epsilon}^P - 2K \frac{\partial K}{\partial T} dT \} / (\frac{\partial F}{\partial \sigma} E^{t+\Delta t} \frac{\partial F}{\partial \sigma}) \end{aligned} \quad (11)$$

and substituting (11) into (4) yields

$$\begin{aligned} d\sigma = E^{t+\Delta t} \{ \{ d\epsilon - [\frac{\partial F}{\partial \sigma} [E^{t+\Delta t} (d\epsilon - d\epsilon^C - d\epsilon^T) + dE(\epsilon^t - \epsilon^P - \epsilon^C - \epsilon^T)]] \\ - \frac{\partial F}{\partial \alpha} d\alpha - 2K \frac{\partial K}{\partial \bar{\epsilon}^P} d\bar{\epsilon}^P - 2K \frac{\partial K}{\partial T} dT \} / (\frac{\partial F}{\partial \sigma} E^{t+\Delta t} \frac{\partial F}{\partial \sigma}) \} \frac{\partial F}{\partial \sigma} \\ - d\epsilon^C - d\epsilon^T \} + dE(\epsilon^t - \epsilon^P - \epsilon^C - \epsilon^T). \end{aligned} \quad (12)$$

Rearranging the last equation to obtain

$$\begin{aligned}
d\sigma &= E^{t+\Delta t} (d\varepsilon - d\varepsilon^C - d\varepsilon^T) + dE(\varepsilon^t - \varepsilon^P - \varepsilon^C - \varepsilon^T) \\
&= \frac{E^{t+\Delta t} \frac{\partial F}{\partial \sigma} \frac{\partial F}{\partial \sigma} E^{t+\Delta t} (d\varepsilon - d\varepsilon^C - d\varepsilon^T)}{\frac{\partial F}{\partial \sigma} E^{t+\Delta t} \frac{\partial F}{\partial \sigma}} \\
&= \frac{E^{t+\Delta t} \frac{\partial F}{\partial \sigma} \frac{\partial F}{\partial \sigma} dE(\varepsilon^t - \varepsilon^P - \varepsilon^C - \varepsilon^T)}{\frac{\partial F}{\partial \sigma} E^{t+\Delta t} \frac{\partial F}{\partial \sigma}} \\
&+ E^{t+\Delta t} \frac{\partial F}{\partial \sigma} \left[\frac{-\frac{\partial F}{\partial \sigma} d\alpha - 2K \frac{\partial K}{\partial \varepsilon^P} d\varepsilon^P - 2K \frac{\partial K}{\partial T} dT}{\frac{\partial F}{\partial \sigma} E^{t+\Delta t} \frac{\partial F}{\partial \sigma}} \right] . \quad (13)
\end{aligned}$$

Using the normality condition (7) one can write

$$-E^{t+\Delta t} \frac{\partial F}{\partial \sigma} = -E^{t+\Delta t} \frac{d\varepsilon^P}{d\lambda} . \quad (14)$$

Then equation (4) can be rewritten as

$$-E^{t+\Delta t} \frac{d\varepsilon^P}{d\lambda} = \frac{d\sigma}{d\lambda} - \frac{1}{d\lambda} [E^{t+\Delta t} (d\varepsilon - d\varepsilon^C - d\varepsilon^T) + dE(\varepsilon^t - \varepsilon^P - \varepsilon^C - \varepsilon^T)] , \quad (15)$$

and equation (13) can also be rewritten as

$$\begin{aligned}
\theta d\sigma &= E^{t+\Delta t} (d\varepsilon - d\varepsilon^C - d\varepsilon^T) \theta - E^{t+\Delta t} \frac{\partial F}{\partial \sigma} \frac{\partial F}{\partial \sigma} E^{t+\Delta t} (d\varepsilon - d\varepsilon^C - d\varepsilon^T) \\
&+ dE(\varepsilon^t - \varepsilon^P - \varepsilon^C - \varepsilon^T) - E^{t+\Delta t} \frac{\partial F}{\partial \sigma} \frac{\partial F}{\partial \sigma} E(\varepsilon^t - \varepsilon^P - \varepsilon^C - \varepsilon^T) , \quad (16)
\end{aligned}$$

where

$$0 = \frac{\partial F}{\partial \sigma} \frac{d\alpha}{d\lambda} + 2K \frac{\partial K}{\partial \varepsilon^P} \frac{d\varepsilon^P}{d\lambda} + 2K \frac{\partial K}{\partial T} \frac{dT}{d\lambda} + E^{t+\Delta t} \frac{\partial F}{\partial \sigma} \frac{\partial F}{\partial \sigma} . \quad (17)$$

Rearrange above to obtain

$$d\sigma = \left[E^{t+\Delta t} - \frac{E^{t+\Delta t} \frac{\partial F}{\partial \sigma} \frac{\partial F}{\partial \sigma} E^{t+\Delta t}}{\theta} \right] (d\varepsilon - d\varepsilon^C - d\varepsilon^T) \\ + \left[dE - \frac{E^{t+\Delta t} \frac{\partial F}{\partial \sigma} \frac{\partial F}{\partial \sigma} dE}{\theta} \right] (\varepsilon^t - \varepsilon^P - \varepsilon^C - \varepsilon^T) \quad (18)$$

Now make the assumption made by Hunsaker [28] that

$$(d\sigma - C d\varepsilon^P) \frac{\partial F}{\partial \sigma} = 0 \quad (19)$$

which defines C as a scaling parameter requiring $(d\sigma - C d\varepsilon^P)$ to be perpendicular to the yield surface outer normal. The verification of this assumption is discussed by Allen [29]. Rewrite equation (8)

$$\frac{\partial F}{\partial \sigma} d\sigma = \frac{\partial F}{\partial \sigma} d\alpha + 2K \frac{\partial K}{\partial \varepsilon} d\varepsilon^P + 2K \frac{\partial K}{\partial T} dT \quad (20)$$

and equate with (19) to obtain

$$C d\varepsilon^P \frac{\partial F}{\partial \sigma} = \frac{\partial F}{\partial \sigma} d\sigma = \frac{\partial F}{\partial \sigma} d\alpha + 2K \frac{\partial K}{\partial \varepsilon} d\varepsilon^P + 2K \frac{\partial K}{\partial T} dT \quad (21)$$

Also, substitute the normality condition (7) into (21) will give

$$Cd\lambda \frac{\partial F}{\partial \sigma} \frac{\partial F}{\partial \sigma} = \frac{\partial F}{\partial \sigma} d\sigma = \frac{\partial F}{\partial \sigma} d\alpha + 2K \frac{\partial K}{\partial \varepsilon} d\varepsilon^P + 2K \frac{\partial K}{\partial T} dT \quad (22)$$

or

$$C \frac{\partial F}{\partial \sigma} \frac{\partial F}{\partial \sigma} = \frac{1}{d\lambda} \frac{\partial F}{\partial \sigma} d\sigma = \frac{\partial F}{\partial \sigma} \frac{d\alpha}{d\lambda} + 2K \frac{\partial K}{\partial \varepsilon} \frac{\partial \varepsilon^P}{d\lambda} + 2K \frac{\partial K}{\partial T} \frac{\partial T}{d\lambda} \quad (23)$$

Using the relations in (23), equation (17) can now be rewritten as

$$d\sigma = C \frac{\partial F}{\partial \sigma} \frac{\partial F}{\partial \sigma} + E^{t+\Delta t} \frac{\partial F}{\partial \sigma} \frac{\partial F}{\partial \sigma} \quad (24)$$

where

$$C = \frac{\frac{\partial F}{\partial \sigma} d\sigma}{d\lambda \frac{\partial F}{\partial \sigma} \frac{\partial F}{\partial \sigma}} = \frac{d\sigma}{d\lambda \frac{\partial F}{\partial \sigma}} \quad (25)$$

Applying (7), the above becomes

$$C = \frac{d\sigma}{d\varepsilon^P} \quad (26)$$

Physically, C is the slope of the uniaxial stress vs. equivalent uniaxial plastic strain diagram during an isothermal load increment.

However, during a nonisothermal load step

$$d\sigma = \frac{\partial \sigma}{\partial \varepsilon^P} d\varepsilon^P + \frac{\partial \sigma}{\partial T} dT = C d\varepsilon^P + \frac{\partial \sigma}{\partial T} dT \quad (27)$$

or

$$C = \frac{d\sigma}{d\varepsilon^P} + \frac{\partial \sigma}{\partial T} \frac{dT}{d\varepsilon^P} = H' + \frac{\partial \sigma}{\partial T} \frac{dT}{d\varepsilon^P} \quad (28)$$

The above statement is required because the uniaxial stress is a function of both the plastic strain history and temperature during nonisothermal loading.

Finally, substitute (24) and (28) into equation (18) to obtain

$$d\sigma = \left[E^{t+\Delta t} - \frac{E^{t+\Delta t} \frac{\partial F}{\partial \sigma} \frac{\partial F}{\partial \sigma} E^{t+\Delta t}}{H' \frac{\partial F}{\partial \sigma} \frac{\partial F}{\partial \sigma} + E^{t+\Delta t} \frac{\partial F}{\partial \sigma} \frac{\partial F}{\partial \sigma}} \right] (d\varepsilon - d\varepsilon^C - d\varepsilon^T)$$

$$\begin{aligned}
& + \left[dE - \frac{E^{t+\Delta t} \frac{\partial F}{\partial \sigma} \frac{\partial F}{\partial \sigma} dE}{H' \frac{\partial F}{\partial \sigma} \frac{\partial F}{\partial \sigma} + E^{t+\Delta t} \frac{\partial F}{\partial \sigma} \frac{\partial F}{\partial \sigma}} \right] (\epsilon^t - \epsilon^P - \epsilon^C - \epsilon^T) \\
& + \left[\frac{E^{t+\Delta t} \frac{\partial F}{\partial \sigma} \frac{\partial F}{\partial \sigma} \frac{\partial \sigma}{\partial T}}{H' \frac{\partial F}{\partial \sigma} \frac{\partial F}{\partial \sigma} + E^{t+\Delta t} \frac{\partial F}{\partial \sigma} \frac{\partial F}{\partial \sigma}} \right] dT. \tag{29}
\end{aligned}$$

Now for the yield surface translation scalar, substitute (6) into (8) and solve for $d\mu$ as follows

$$\frac{\partial F}{\partial \sigma} d\sigma - \frac{\partial F}{\partial \sigma} [d\mu(\sigma - \alpha)] = 2K \frac{\partial K}{\partial \epsilon^P} + 2K \frac{\partial K}{\partial T} dT \tag{30}$$

$$d\mu \frac{\partial F}{\partial \sigma} (\sigma - \alpha) = \frac{\partial F}{\partial \sigma} d\sigma - 2K \frac{\partial K}{\partial \epsilon^P} d\epsilon^P - 2K \frac{\partial K}{\partial T} dT \tag{31}$$

$$d\mu = \frac{\frac{\partial F}{\partial \sigma} d\sigma - 2K \frac{\partial K}{\partial \epsilon^P} d\epsilon^P - 2K \frac{\partial K}{\partial T} dT}{\frac{\partial F}{\partial \sigma} (\sigma - \alpha)} \tag{32}$$

An outline for the uniaxial computer program utilizing the above equations is contained in the Appendix.

Yield Function

The von Mises yield criterion is used herein and can be written in terms of principal stresses σ_1 as

$$F(\sigma_1) = \frac{1}{2} \{ (\sigma_1 - \sigma_2)^2 + (\sigma_2 - \sigma_3)^2 + (\sigma_3 - \sigma_1)^2 \} = K^2 \tag{33}$$

where K represents the current yield surface size. It has been shown to be in excellent agreement with experiment for many ductile metals,

for example aluminum, cold-worked mild steel, medium carbon and alloy steels [2]. The von Mises yield criterion can be written in uniaxial form (with the use of a combined isotropic-kinematic hardening law) as

$$F(\sigma - \alpha) = (\sigma - \alpha)^2 = K^2 \quad (34)$$

where α is the yield surface center.

Note that the assumed yield function is dependent only on the second deviatoric stress invariant, i.e., independent of hydrostatic stress and with the assumption of initially isotropic materials. Also, the temperature dependence is handled through thermally dependent material properties and is isotropic in nature, but there is no rate dependence in this form of the yield function.

Hardening Rule

Laws governing the influence of plastic deformation on the yield surface and strain hardening of a material are called hardening rules. A significant amount of research has been done in this area, and there are many different rules in use.

Consider Fig. 2 as a comparison of several hardening rules for a given isothermal load history. Although isotropic hardening will successfully model loading histories in which stress reversals do not occur, it is not satisfactory to model the Bauschinger effect or cyclic phenomenon. Conversely, kinematic hardening will model the Bauschinger effect, but neither hardening rule predicts the increased strain hardening upon reyield as their "square" hysteresis loop predictions show. Oak Ridge (ORNL) [30] and combined hardening rules predict overall

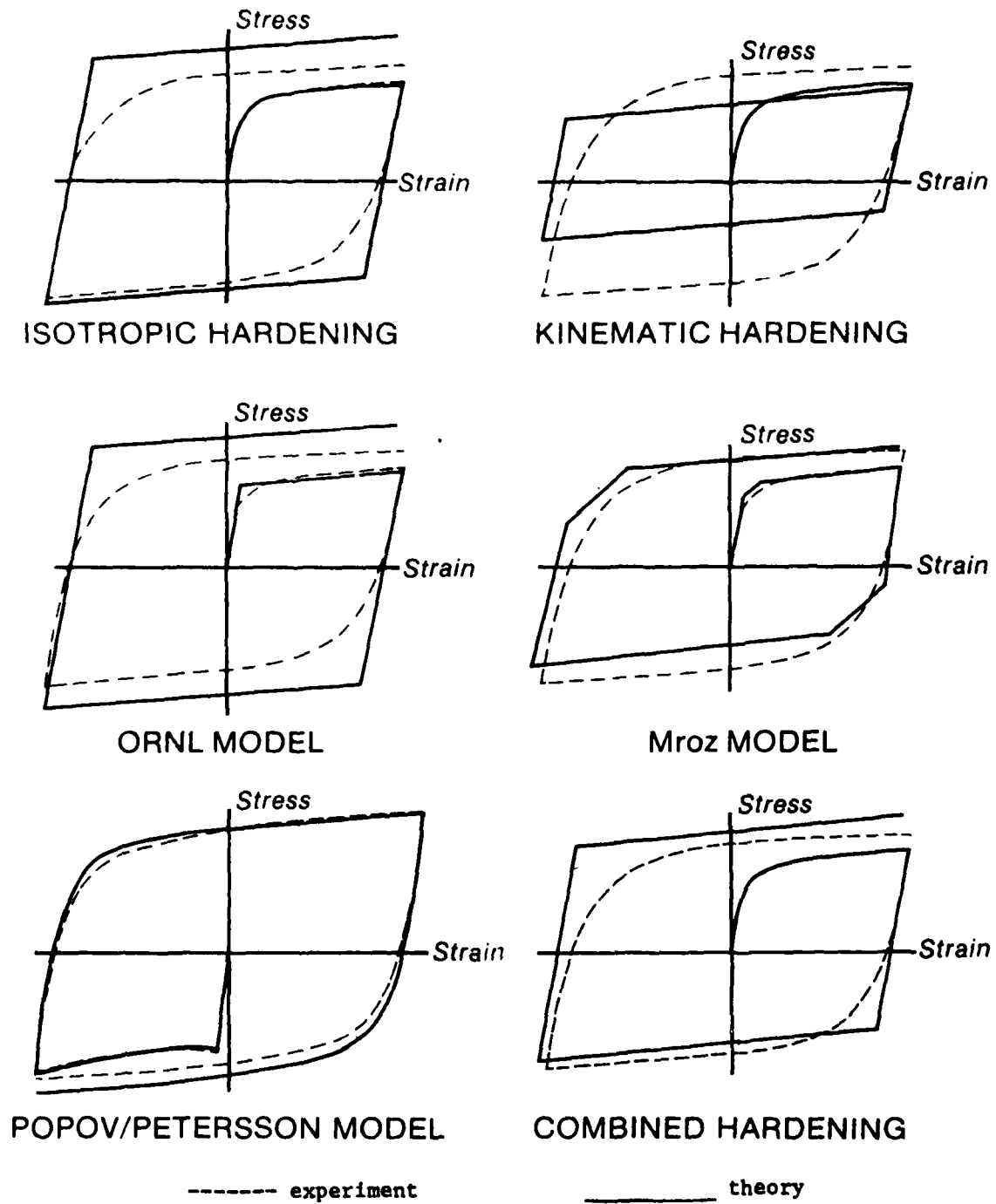


Fig. 2 Plasticity models

response somewhat better. Hunsaker [13] suggests the mechanical sub-layer model for loadings in which stress reversals may occur. Of all the plasticity models displayed in Fig. 2, the multisurface approach of Petersson and Popov [20,21] clearly gives the best theoretical representation of the experiment.

Thus, if one is interested in the exact stress-strain behavior over the entire load history and not just an end result, a hardening law which accounts for increased strain hardening upon reyield becomes a necessity.

At temperatures below roughly one-half the melting point for many metals, a change of loading direction in stress space plays a very important role. In many hardening rules emphasis is placed on how to describe the evolution of the yield surface while little has been done as to how the plastic modulus is affected by stress reversals in cyclic loading [31]. Above this temperature the stress-strain behavior is controlled by rate dependent deformation and experimentally observed hysteresis loops are relatively "square". Thus the simulation of the strain hardening is not as critical.

Many authors mention the "oversquareness" of predicted hysteresis loops. Among these are Miller [16], Dafalias and Popov [31], Walker [9], and Popov and Petersson [20,21]. It seems that this phenomenon is of some interest to the researchers in this field. Miller improves his unified time-dependent constitutive equations by making the kinematic work-hardening coefficient a function of the back stress and the sign of the nonelastic strain rate and shows favorable agreement with that observed in 2024-T4 aluminum alloy. Another approach by

Dafalias and Popov which was extended by Petersson and Popov involves enclosing the initial yield surface within a larger bounding surface. Both surfaces are allowed to translate and deform in stress space, and the proximity of the two determines the plastic moduli. Two other hardening rules which provide for a high strain-hardening rate upon reyielding are the Mroz and mechanical sublayer models [13].

Since Miller's theory [16] is microphenomenologically based, he seeks to make his model consistent with existing microphysical explanations. He states that dislocations moving in a given direction will form dislocation loops by interaction with precipitate particles, and when the direction of dislocation motion is reversed a dislocation can annihilate a nearby loop which was previously left behind. A relatively rapid change of strain in the nature of the stress field encountered by the reversing dislocation would result and lead to a large value of the slope $d\sigma/d\epsilon$. As the strain continues to reverse, dislocations will no longer be encountering such oppositely-signed loops and $d\sigma/d\epsilon$ will gradually decrease. Miller models this by associating the directionality of the dislocation debris with the back stress R and the direction of current dislocation motion with the sign of the difference $\sigma/E-R$. A similar argument is given by Polakowski and Rippling [14].

Although the combined isotropic-kinematic hardening rule used by Allen and Haisler [25] cannot represent the high rate of strain hardening accompanying stress reversals which cause yielding, it does account for thermally dependent material properties and the Bauschinger effect. Thus it was felt that with some modifications, all cyclic characteristics could be modeled. To summarize, the two important

shortcomings of their hardening law in representing cyclic behavior are its failure to account for the high rate of strain hardening upon reyielding after a stress reversal and cyclic saturation.

In terms of actual modelling of the two shortcomings discussed above, several revisions and improvements have been added to the model. First as discussed in regards to experimental data requirements, additional stress-strain input is required to characterize various strain hardening rates. Metals like aluminum exhibit a similar strain hardening behavior for reyield after the initial yield. Conversely, stainless steel can exhibit two different forms of hardening behavior even after several loading cycles. A program flag controls which input stress-strain curve to use to generate hardening parameters depending on the material being modeled and the yield (load) history. Secondly, the hardening ratio was allowed to be a function of plastic strain and in some cases the direction of loading. This allows modelling of cyclic saturation.

More specifically, the hardening rule revisions can be explained in two different discussions. The first deals with strain hardening upon reyield and the second with cyclic saturation.

Use of the combined hardening law in Allen and Haisler [25], predicts cyclic behavior like that shown in Fig. 3. The hardening ratio, β is the ratio of isotropic to kinematic hardening. Setting $\beta=0$ constitutes a kinematic hardening law where the yield surface retains its initial size, shape, and orientation thus simply translating in principal stress space. Isotropic hardening, $\beta=1$, means that during plastic flow the yield surface expands uniformly about the origin and

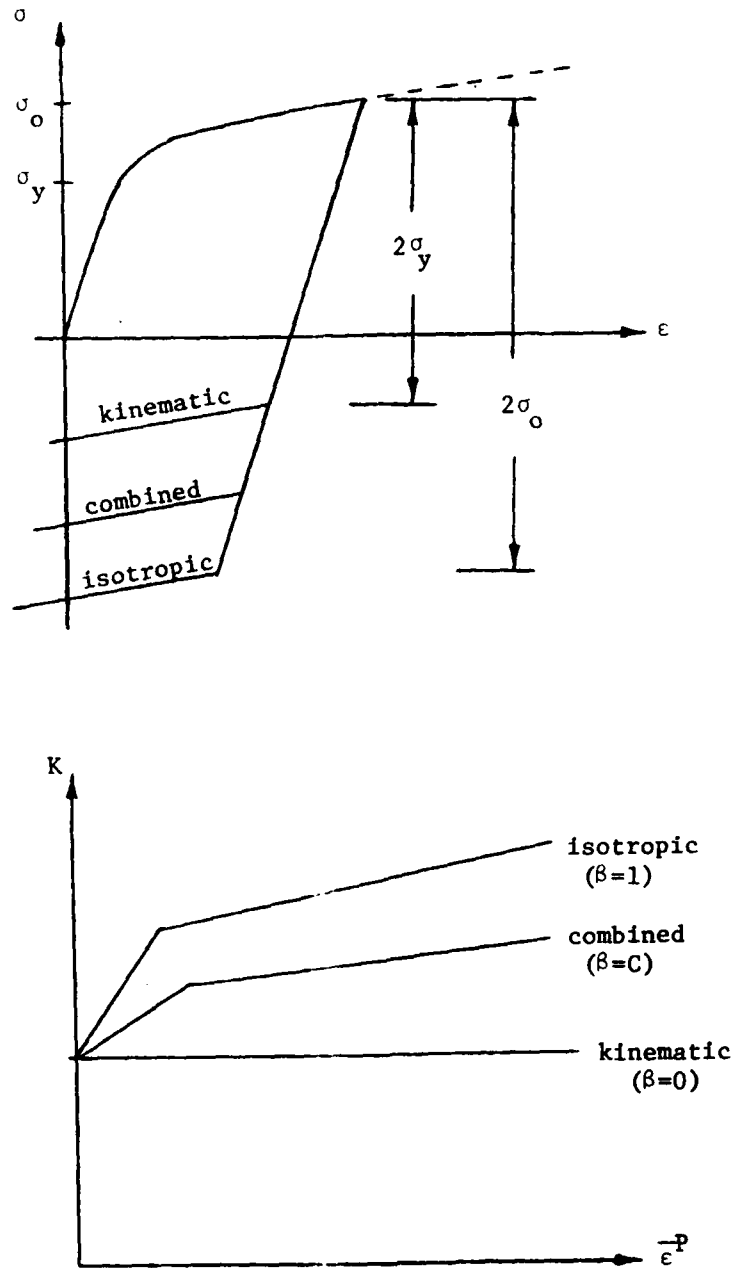


Fig. 3 Definition of standard hardening rules

never translates. Using a value for the hardening ratio such as $0 \leq b \leq 1$ constitutes a combined hardening rule where the yield surface is allowed to both expand and translate.

Notice in Fig. 3 that the reyielded strain hardening behavior is "squared-off" as discussed above. The revised model has the ability to reproduce strain hardening behavior that is dependent on direction or history of yielding. This is observed in experiment as the high rate of strain hardening upon stress reversal in a cyclic load test. In other words, the material demonstrates two distinct forms of behavior as shown in Fig. 4. Initial strain hardening character is usually quite "sharp" in comparison with the rounded shape of the reverse loading curve. Popov and Petersson [21] found it essential in dealing with cyclic steel behavior to use two stress-strain curves as input. The first is from a monotonic test on virgin material and the second is from a hysteresis loop which develops after several loading cycles.

For a large number of common metals, a cyclic load history leads to a limiting periodic response in which the stress-strain curve for each consecutive cycle is the same. This is termed cyclic saturation and is illustrated in Fig. 5 [32]. Capability to portray this phenomenon is not contained in many common hardening laws. With the addition of a hardening ratio that is a function of plastic strain and in some cases direction of loading into the existing model, this phenomenon can be modeled much more successfully than a combined hardening rule with a constant hardening ratio.

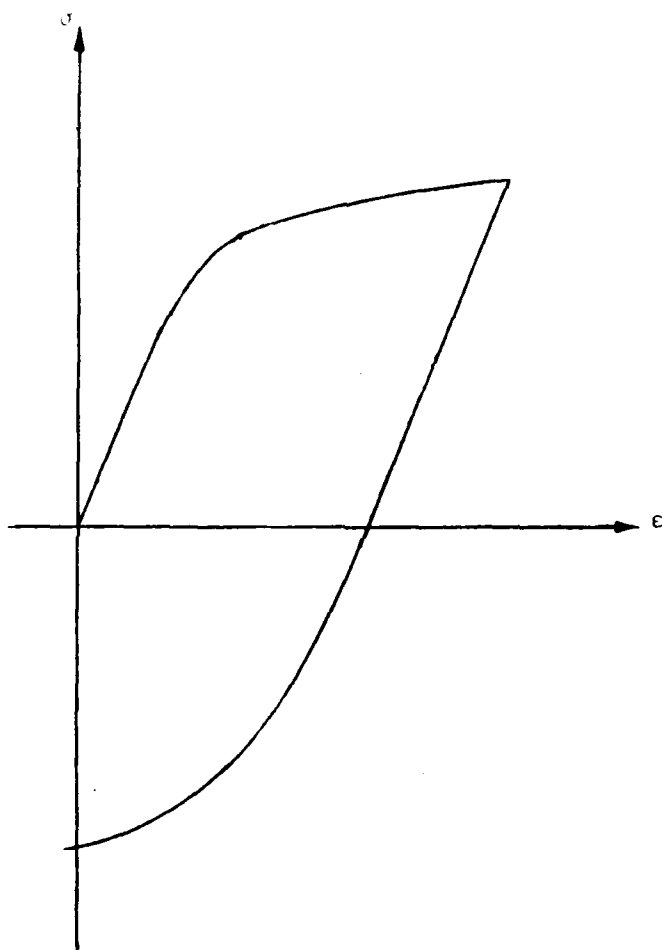


Fig. 4 Typical experimental results showing difference in first and second quarter cycle response

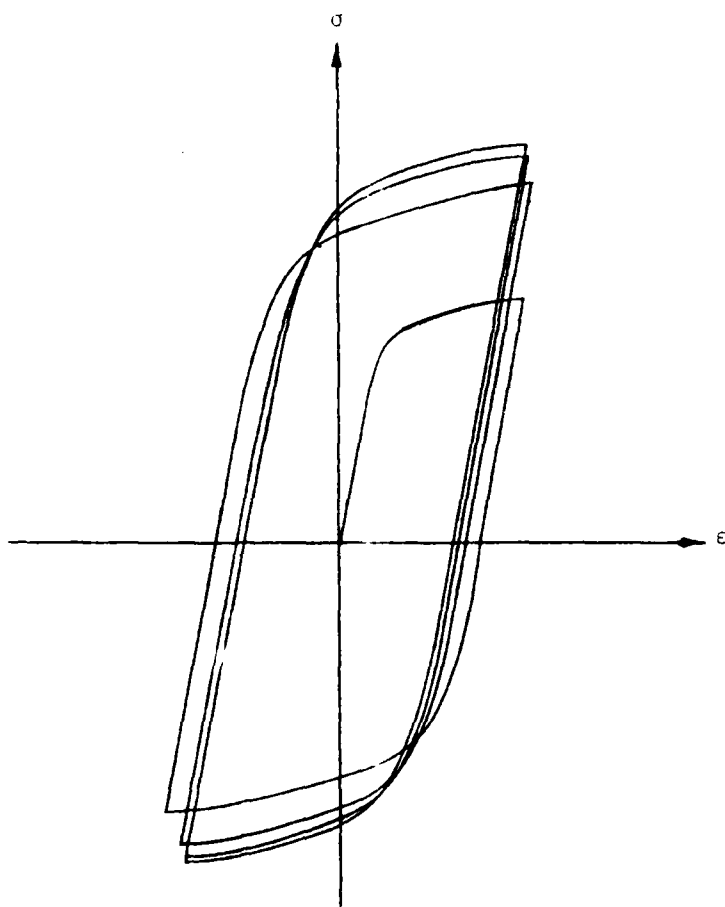


Fig. 5 Mechanical response of typical ductile metal exhibiting cyclic saturation in cyclic loading

The reader is referred to the sections on experimental data requirements and theoretical examples for more details concerning the above discussion.

Creep Strain Increment

The creep strain is defined as the uncoupled rate dependent inelastic deformation in the present theory. Several methods are available to characterize this strain component. Traditional characterization has been based on the use of standard creep tests run at constant stress and temperature. Creep strain (or creep strain rate) is written as a function of time, stress, and temperature through the use of power law functions, exponentials, hyperbolic functions, etc. obtained by appropriate curve fitting techniques. Additional ad hoc creep hardening rules have been devised to model rate dependent behavior during reverse and cyclic loading. Oak Ridge National Laboratory used such models for 304 stainless steel with some success [33]. In many cases it is more expedient to use tabulated creep strain data as opposed to curve fitted data; although this requires numerical interpolation between a set of isothermal, constant stress creep curves.

In the present research, an alternate approach has been taken involving hysteresis loops and stress relaxation tests at various temperatures. Fig. 6 shows a typical set of these tests and details how the rate dependent deformation is extracted from them.

A reference temperature hysteresis loop is defined at a temperature below which the total strain consists essentially of elastic and rate independent plastic strains only. Above this temperature, the

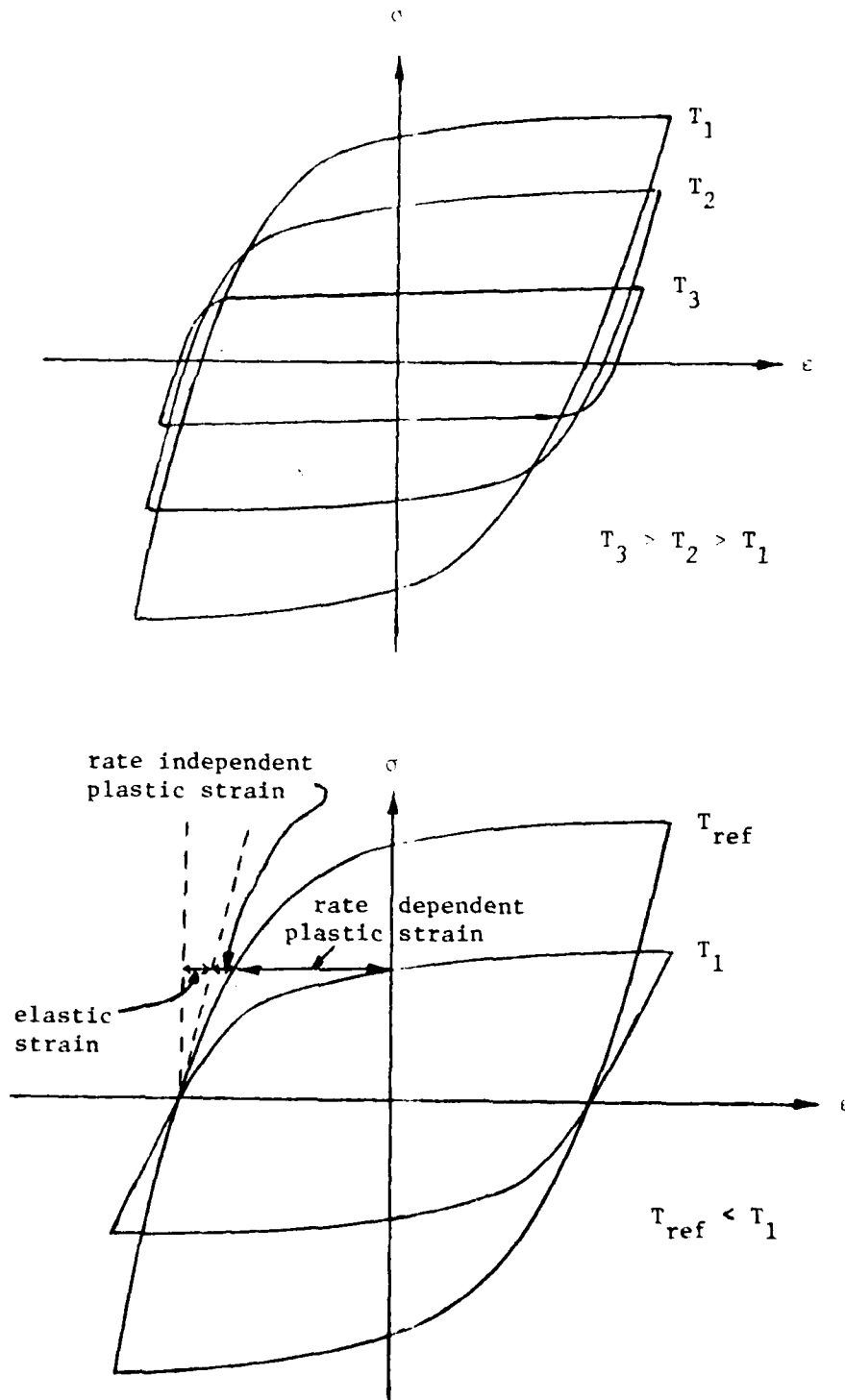


Fig. 6 Experimental characterization of the rate dependence of the model

rate dependent inelastic strain (creep) dominates. Experimentally, Bradley and Haisler [34,35] have shown for Hastelloy-X that such an uncoupling appears feasible.

Micromechanical considerations suggest a model for the rate dependent inelastic strain of the form

$$\dot{\epsilon}^C = \left(\frac{\sigma - \Omega}{K_0} \right)^n, \quad (35)$$

where $\dot{\epsilon}^C$ represents the rate dependent inelastic strain rate, Ω is the back stress, K_0 is the drag stress, and n is a constant. The back stress, drag stress, and exponent n are generally functions of temperature and strain. However, for some materials a good assumption is that the drag stress and n are constant at sufficiently high temperatures.

At the tips of the hysteresis loops, the stress and back stress have reached maximum values σ_{\max} and Ω_{\max} respectively. If we let σ_1 and σ_2 denote the maximum stress values at two different strain rates $\dot{\epsilon}_1$ and $\dot{\epsilon}_2$, then the value of n can be computed as

$$n = \ln(\dot{\epsilon}_1 / \dot{\epsilon}_2) / \ln[(\sigma_1 - \Omega_{\max}) / (\sigma_2 - \Omega_{\max})] \quad (36)$$

where Ω_{\max} is assumed to be constant between $\dot{\epsilon}_1$ and $\dot{\epsilon}_2$. Similarly, the constant K_0 can be determined by rewriting (35) in the form

$$K_0 = (\sigma_1 - \Omega_{\max}) \dot{\epsilon}_1^{-1/n}. \quad (37)$$

It should be noted that a number of the unified models reviewed in Chapter II (for example, Walker's [9]) utilized similar functional

forms and experimental characterizations of the inelastic strain component compared to that used in this research for rate dependent inelastic strain. Although the functional forms used to model the unified inelastic strain give excellent agreement at high temperature (where rate dependence dominates), they give overly square stress-strain response at low temperature (where rate independent plasticity dominates). This is due primarily to the failure of the present unified models to account properly for rate independent behavior. In the present research, this difficulty is hopefully overcome by modeling the rate dependent inelastic and rate independent inelastic strain more accurately with appropriate definition of a temperature range where each is applicable.

Experimental Data Requirements

One of the requirements for a good constitutive model is that it have reasonable experimental data requirements. Characterization of model parameters should follow easily from standard tests.

All experimental data tests are performed at sufficient levels of the primary variables (strain and temperature) in order to bracket their magnitudes in the particular test of interest. Consideration is also given to allow accurate linear interpolation between temperatures.

The first set of tests required is uniaxial isothermal single cycle reverse loading tests like those shown in Fig. 7. These tests are performed at fast enough strain rates so that the rate dependent component of deformation is negligible. Characterization of both

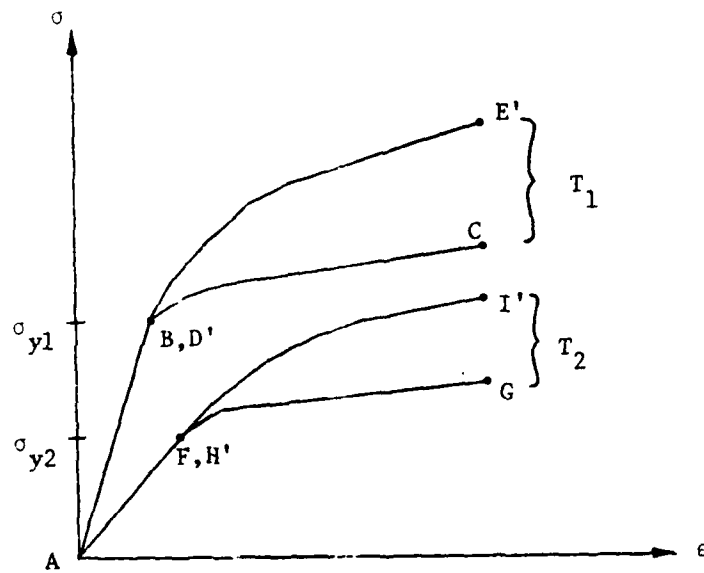
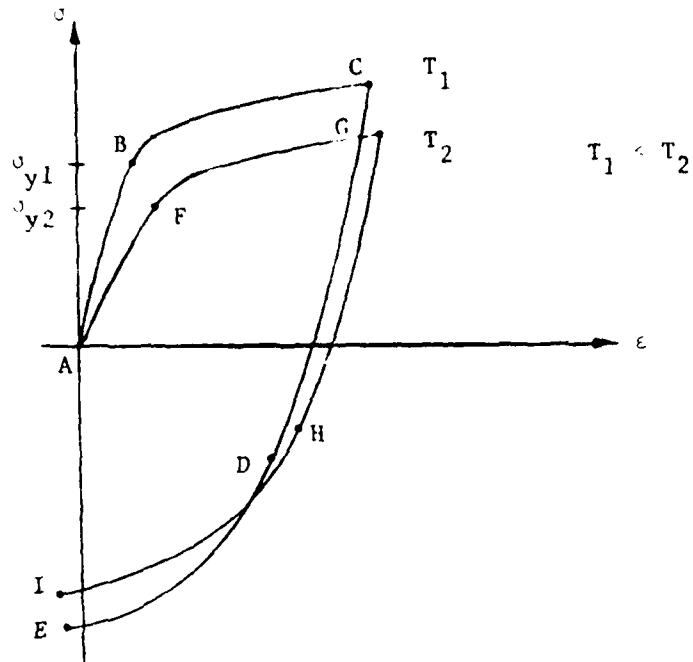


Fig. 7 Uniaxial isothermal single cycle reverse loading curves and their linear representations input to the model

initial and subsequent strain hardening behavior is the reason for the reverse loading tests. Piecewise linear representations of the data obtained from experiment are input into the model with the number of linear segments used depending on the accuracy desired.

For example as shown in Fig. 7 at $T=T_1$, the initial elastic-plastic behavior is characterized by curve ABC. Similarly the subsequent elastic-plastic behavior is characterized by curve DE. The piecewise linear representations become curve ABC and D'E' where D'E' was obtained by shifting curve DE to the yield point B. A similar procedure is performed for all other temperatures as required. Note that if the difference in strain hardening behavior is not considered critical, (the difference between curves ABC and DE is insignificant) only curves ABC and AFG would be required input.

If the hardening ratio is constant with respect to plastic strain, it can also be determined from the above tests using the relation

$$\delta = \frac{\sigma_r - (2\sigma_y - \sigma_o)}{(2\sigma_o - 2\sigma_y)}, \quad (38)$$

where stress values are defined in Fig. 8 for each temperature. If δ is a function of plastic strain as well as temperature, several cycles of stress-strain data would be required to characterize this parameter. Typical input curves for the hardening ratio are also shown in Fig. 8.

A piecewise linear description of the temperature dependence of the coefficient of thermal expansion is also required if it varies significantly for the temperature range of interest.

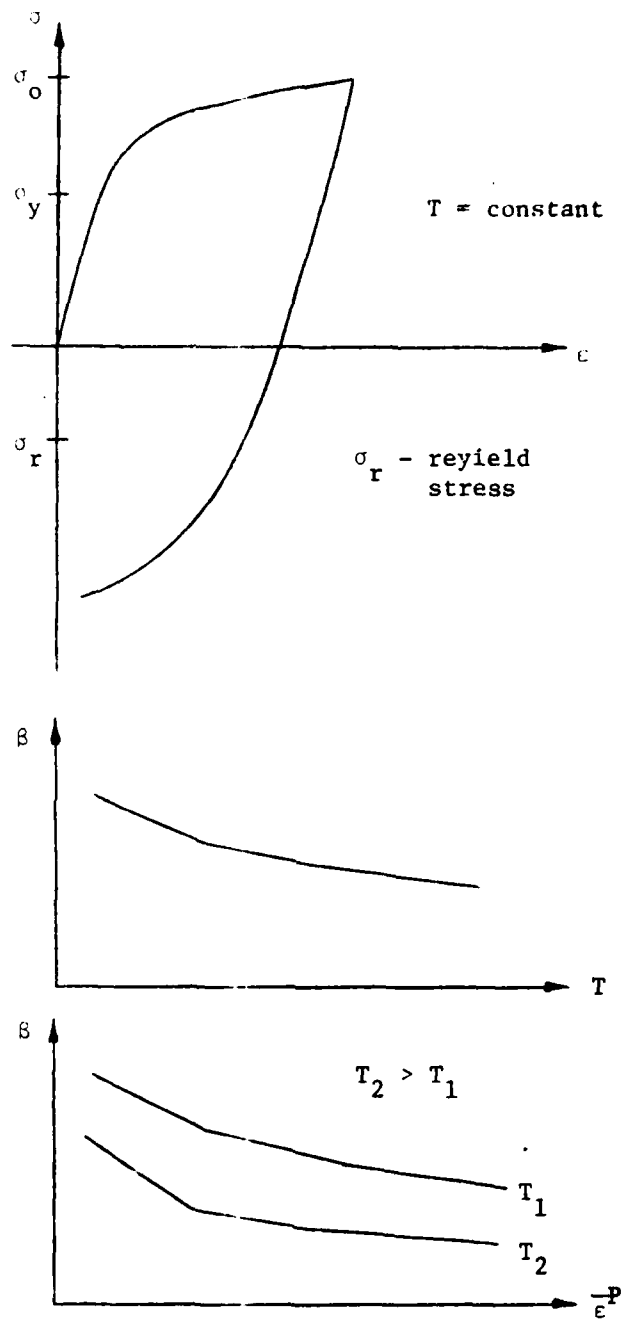


Fig. 8 Hardening ratio

Experimental characterization of the rate dependent terms is the same as for Walker's model [9]. Steady state hysteresis loops at different strain rates under fully reversed strain controlled conditions as shown previously in Fig. 6 (p. 30) are required. These are all performed until saturated values are established. Also required are stress drop creep and relaxation tests from initial point on a steady state hysteresis loop. All constants are a function of temperature and require the above tests to be performed at all temperatures of interest unless interpolation is used.

For comparative purposes, a brief description of the experimental data requirements for several other constitutive models is presented.

The first tests required by Krieg, et al. [11] are stress-drop tests during steady state creep. This means that a fraction of the applied stress is removed rapidly, and then this reduced stress is held constant until the accrued strain is sufficient to permit the strain rate immediately after the drop to be obtained by extrapolation. The stress is then increased to its original value to re-establish steady state creep. This procedure allows the response of a specimen to drop tests of various magnitudes to be obtained from a single creep stress. For full characterization, this test procedure must be repeated at several nominal creep stress levels and temperatures. Steady state and primary creep data must also be utilized.

Miller [16] states that with a general purpose constitutive equation a fairly wide variety of data is required. Calculation of a complete set of material constants for an alloy on which hysteresis loop data are available can be a very lengthy task with a substantial

amount of experimentation required for his model.

The characterization of model parameters for the theory of Bodner, et al. [15] requires two monotonic stress-strain curves at different steady strain rates. For cyclic loading an additional constant is required, but determination of that constant is unclear in their presentation.

Construction of Yield Surface Size and Stress vs. Equivalent Uniaxial Plastic Strain Diagrams

Calculation of the yield surface size and equivalent uniaxial stress is accomplished by constructing K and $\bar{\sigma}$ vs. $\bar{\epsilon}^P$ diagrams and interpolating on these diagrams at known values of $\bar{\epsilon}^P$ and T . From a piecewise linear representation of a "zero time" stress-strain curve, the equivalent uniaxial plastic strain is given by

$$\bar{\epsilon}_i^P = \epsilon_{x_i} - \sigma_{x_i} / E \quad (39)$$

The yield surface size and equivalent uniaxial stress are given by

$$K_i = \sigma_y + \beta(\sigma_{x_i} - \sigma_y) \quad (40)$$

$$\bar{\sigma}_i = \sigma_{x_i} \quad (41)$$

where σ_y represents the yield stress.

For the revised hardening law, two each of the above diagrams are required. The first diagrams for each case (K and $\bar{\sigma}$) will be labeled base diagram and are simply the functions calculated from equations (39) - (41) for the input stress-strain curves. These change only if

the hardening ratio is a function of plastic strain. The second set or global diagrams evolve throughout the solution process. They are initialized to equal the base diagrams but are modified each time a load reversal which causes yielding occurs. The modification process consists of linking the base curves to the global curves at the values of $\bar{\epsilon}^P$, K and $\bar{\sigma}$ corresponding to the yield stress of interest. Inputting two stress-strain curves at each temperature comes into play as there exists for example two K vs. $\bar{\epsilon}^P$ base diagrams at each input temperature. Factors such as type of material and load history determine which base curve is linked to the global diagram. All program interpolation for calculation of model parameters is done on the global diagrams.

The above procedure is best explained by a figurative example. Using Fig. 7 (p. 33) as the input stress-strain curves, the K vs. $\bar{\epsilon}^P$ base diagram for a constant hardening ratio is shown at the top of Fig. 9. Recall that the "a" curves are the ones that result from reverse yielding while the "b" curves are from the virgin stress-strain curves. Note that the Allen and Haisler model uses only the "b" curves. A reverse yielding occurs at $\bar{\epsilon}^P = \bar{\epsilon}_0^P$ causing the "b" curves to be linked to the global diagram as shown at the bottom of Fig. 9. When another reverse yielding takes place, either the "a" or "b" curves are linked to the global diagram at that particular value of $\bar{\epsilon}^P$. A similar procedure is carried out for the global $\bar{\sigma}$ vs. $\bar{\epsilon}^P$ diagram.

Computational Considerations

For completeness of the theoretical presentation, the gradients, transition step, thermal strain increment, and elastic strain

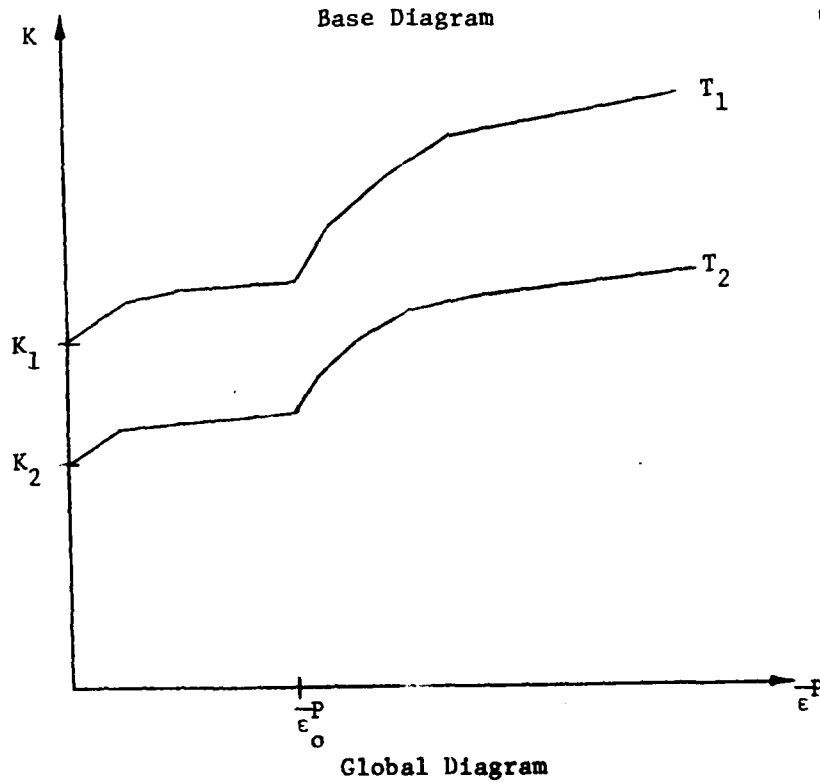
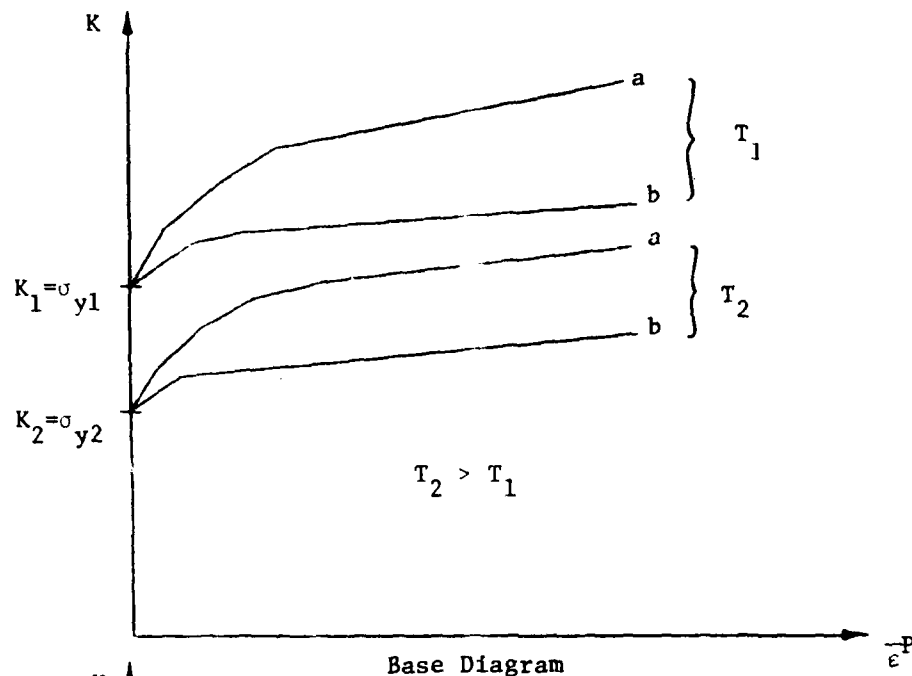


Fig. 9 Construction and evolution of K vs. $\frac{-P}{\epsilon}$ diagrams

increment are all discussed below with regards to computational considerations. They are also presented by Allen [36].

Gradients. Linear interpolation is performed to compute values between input temperatures. The yield surface temperature gradient can be obtained by

$$\frac{\partial K}{\partial T} = \frac{K_H - K_L}{T_H - T_L} \quad (42)$$

where the subscripts H and L denote the values of a particular variable for the temperatures above and below the current temperature T.

Similarly

$$\frac{\partial \bar{\sigma}}{\partial T} = \frac{\bar{\sigma}_H - \bar{\sigma}_L}{T_H - T_L} \quad (43)$$

where the stress values are obtained from the $\bar{\sigma}$ vs. $\bar{\epsilon}^P$ diagram. The slope of the K vs. $\bar{\epsilon}^P$ diagram can be obtained by

$$\frac{\partial K}{\partial \bar{\epsilon}^P} = \left(\frac{\partial K}{\partial \bar{\epsilon}^P} \right)_H - \left\{ \left(\frac{\partial K}{\partial \bar{\epsilon}^P} \right)_H - \left(\frac{\partial K}{\partial \bar{\epsilon}^P} \right)_L \right\} \frac{(T_H - T)}{(T_H - T_L)} \quad (44)$$

and the slope of the $\bar{\sigma}$ vs. $\bar{\epsilon}^P$ diagram by

$$H' = (H')_H - \left\{ (H')_H - (H')_L \right\} \frac{(T_H - T)}{(T_H - T_L)} \quad (45)$$

Transition step. Special treatment must be given to the transition step from elastic to elastic-plastic behavior. The portion of the assumed elastic stress increment $d\sigma$ which will cause yielding is $\zeta d\hat{\sigma}$ and the strain increment to bring the total strain to the

yield surface is $n d\epsilon$. Thus for the transition step, the stress and strain status are modified to become

$$\sigma \rightarrow \sigma + \zeta d\hat{\sigma} \quad (46)$$

$$\epsilon \rightarrow \epsilon + n d\epsilon \quad (47)$$

where

$$\zeta = \frac{-B + \sqrt{B^2 - 4AC}}{2A} \quad (48)$$

$$A = d\hat{\sigma} d\hat{\sigma}$$

$$B = 2(\sigma - \alpha) d\hat{\sigma} \quad (49)$$

$$C = (\sigma - \alpha)(\sigma - \alpha) - (K^{t+\Delta t})^2$$

$$\eta = \frac{\sigma^t + \zeta d\hat{\sigma} - E^{t+\Delta t} \epsilon^t}{E^{t+\Delta t} d\epsilon^t} \quad (50)$$

The above equations are presented here for completeness of the theory.

A full derivation of them is given by Allen [12].

Thermal and elastic strain increments. The thermal strain increment is given by [36]

$$d\epsilon^T = \alpha_T^{t+\Delta t} (T_{t_2} - T_R) - \alpha_T^t (T_{t_1} - T_R), \quad (51)$$

where $\alpha_T^{t+\Delta t}$ and α_T^t are the coefficients of thermal expansion at the beginning and end of a load step respectively, T_{t_1} and T_{t_2} are the temperatures at the beginning and end of a load step respectively, and T_R is the reference temperature for the unstrained state.

The elastic strain increment is calculated by [36]

$$d_t E = \frac{1}{E^{t+\Delta t}} \{d\sigma - dE(\epsilon^t - \epsilon^t - \epsilon^t - \epsilon^t)\} \quad (52)$$

Extension to Multiaxial Theory

The approach used to derive the uniaxial constitutive equations makes it very simple to extend them to the multiaxial case. For example, equation (29) could be simplified considerably by, for instance, dividing out terms like $\partial F/\partial \sigma$. This is not done, however, to retain generality and ease of extension to the multiaxial case. To convert equation (29) to a three dimensional form simply let uniaxial values of stress and strain become the respective stress and strain tensors. Recall the yield function is stated in terms of principal stresses in equation (33). The general elastic constitutive matrix is then substituted for the elastic modulus.

Gradients are still determined from uniaxial input stress-strain data, in fact the only additional experimental data required is Poisson's ratio. The equivalent uniaxial plastic strain is

$$d\bar{\epsilon}^P = \frac{2}{3} d\epsilon_{ij}^P d\epsilon_{ij}^P \quad (53)$$

in tensor notation. In engineering notation this equation can be written as

$$d\bar{\epsilon}^P = \left\{ \frac{2}{9} [(d\epsilon_x^P - d\epsilon_y^P)^2 + (d\epsilon_y^P - d\epsilon_z^P)^2 + (d\epsilon_z^P - d\epsilon_x^P)^2 + 6(d\epsilon_{xy}^P)^2 + 6(d\epsilon_{xz}^P)^2 + 6(d\epsilon_{yz}^P)^2] \right\}^{1/2} \quad (54)$$

A full derivation of the multiaxial theory is contained in reference [12].

CHAPTER IV

EVALUATION OF THE MODEL

Evaluation of the constitutive model detailed in this thesis is now performed. A section on theoretical model capabilities is presented followed by evaluation against experiment.

Theoretical Model Capabilities

Several examples of the capabilities of the model proposed by Allen and Haisler are given in references [36] for the uniaxial case and [12] for the multiaxial case. The purpose of the following examples is to demonstrate the improvements in the revised model by using theoretical illustrations of experimentally observed behavior.

Example 1 - Change of strain hardening with stress reversal. The revised model has the ability to reproduce strain hardening behavior that is dependent on direction of yielding. Fig. 10 illustrates the input stress-strain curves for a theoretical single cycle reverse load test. The input can be taken from either first or saturated cycle data. On the input diagram curve B represents the initial strain hardening behavior while curve A represents the high rate of strain hardening seen upon stress reversal. If a single cycle reverse load test is performed with this theoretical data, the results will be similar to those shown as output in Fig. 10. The revised model using curves A and B is a much more realistic representation of actually observed experimental behavior for many metals than the combined hardening rule of Allen and Haisler. Even the revised model

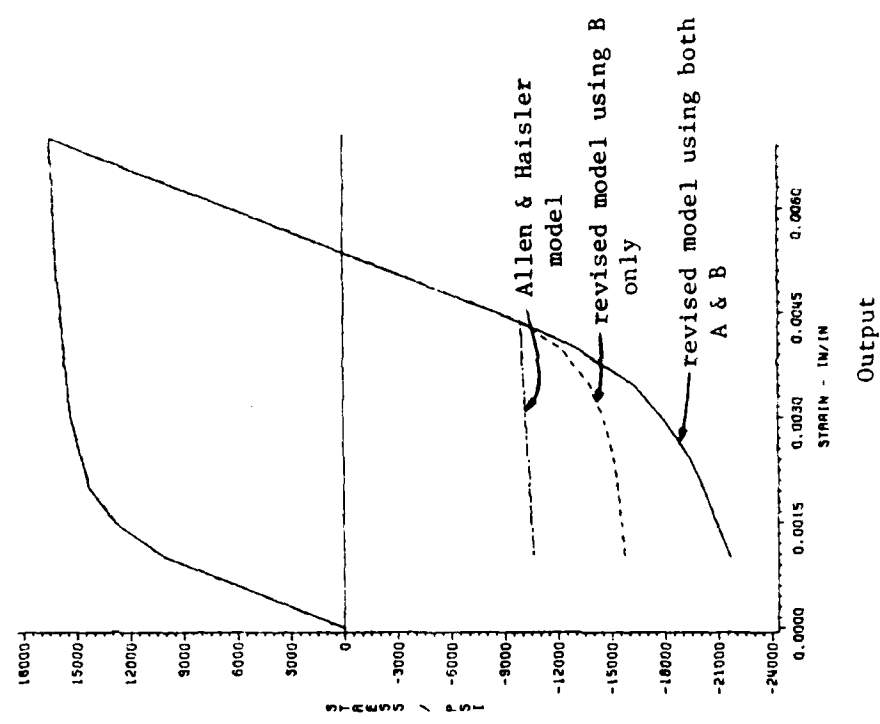
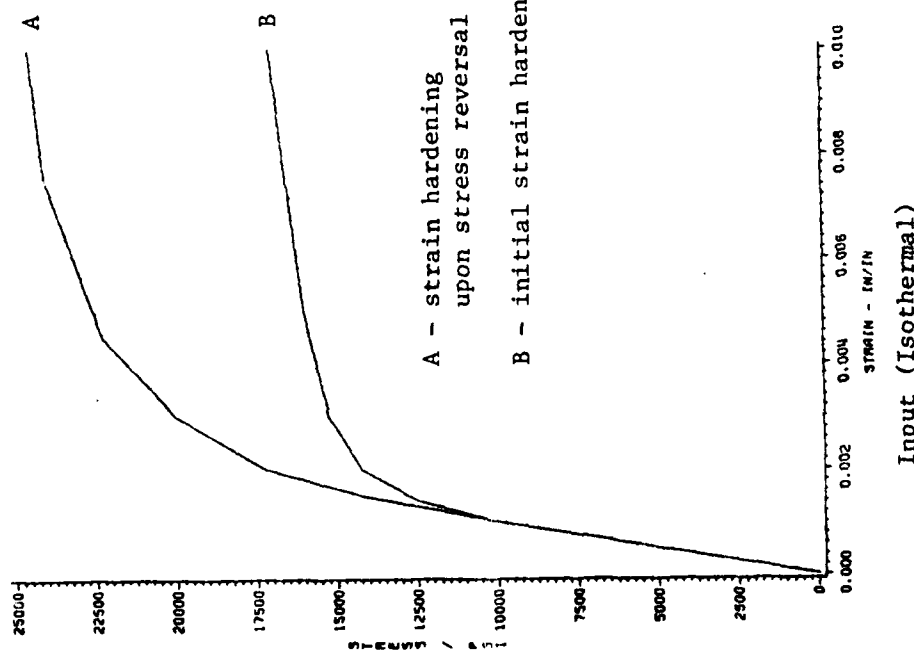


Fig. 10 Change of strain hardening with stress reversal

representation using only curve B is an improvement over existing hardening rules which "square-off" the behavior upon reyield.

Example 2 - Cyclic saturation. A hypothetical fully reversed cyclic strain history of + 0.25% strain was considered using four different values for the hardening ratio. The values used are shown in Fig. 11 following the discussion on hardening rules in Chapter III. An allowance for cyclic saturation is made by letting R be a function of plastic strain. This corresponds physically to allowing the yield surface to first translate and expand and then gradually saturate to a constant size as observed in experiment. Input stress-strain data is the same as the first one-quarter cycle input.

The results for isotropic and kinematic hardening are shown in Fig. 12. Kinematic hardening will model the limiting periodic response, but there is no cyclic hardening of the material in achieving the saturated hysteresis loop. Conversely, isotropic hardening predicts that the material will eventually cycle to a limiting purely elastic response as the yield surface expands without bound. This same behavior is also predicted by a combined hardening law using a constant hardening ratio. It takes somewhat longer to cycle to the elastic response because of the component of kinematic hardening present. This is shown in Fig. 13.

Successful modelling of cyclic saturation is accomplished by letting the hardening ratio in the combined hardening law be a function of plastic strain. For this example, the linear relationship shown in Fig. 11 was assumed with results as shown in Fig. 13. Both the cyclic hardening and limiting periodic responses are depicted.

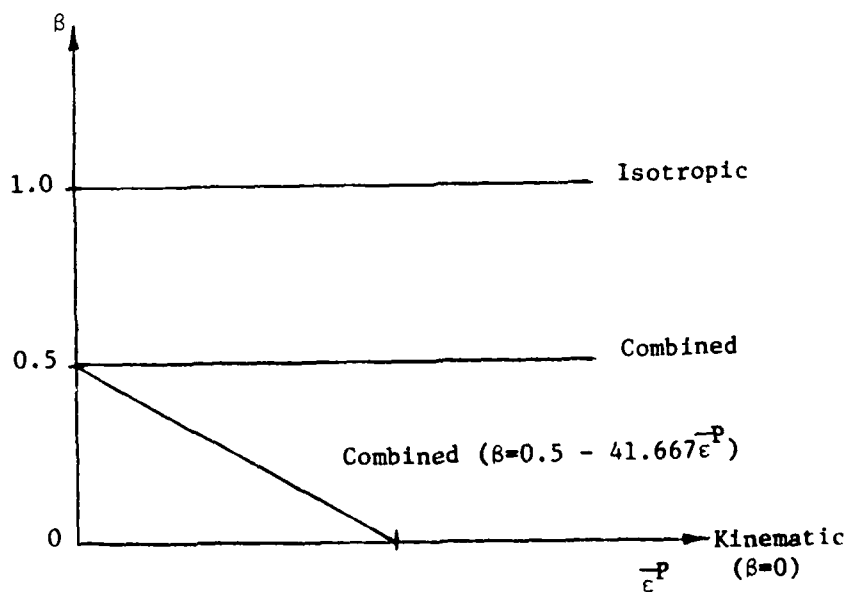
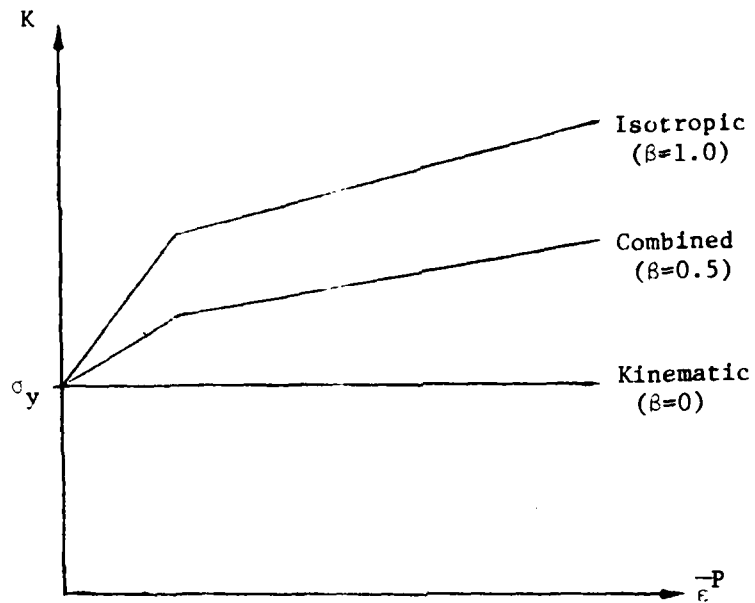
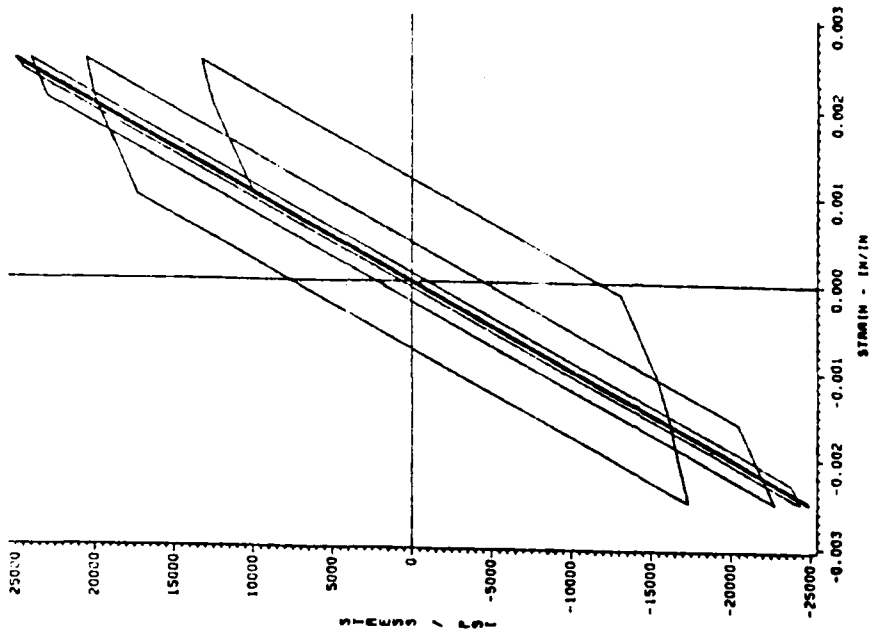
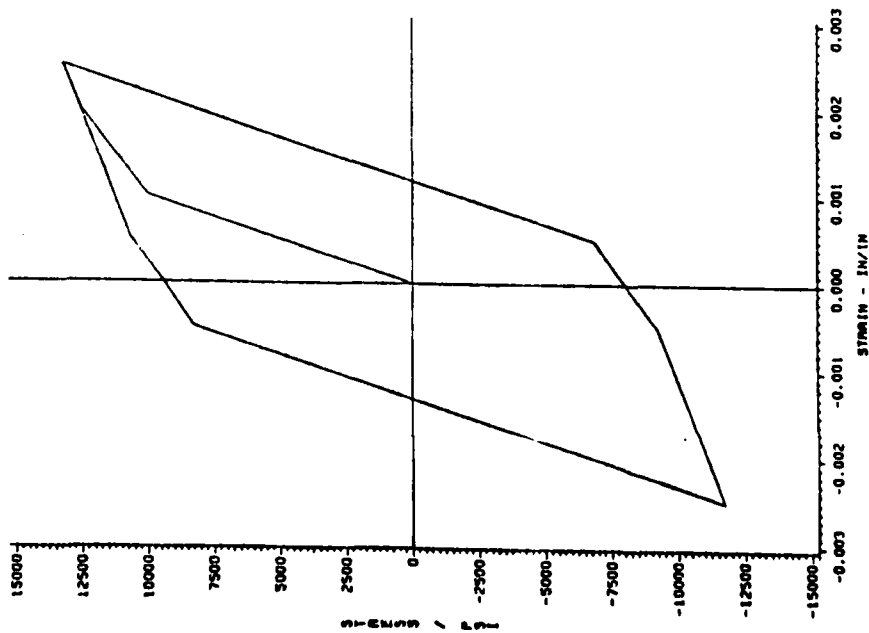


FIG. 11 Hardening rules used in Example 2

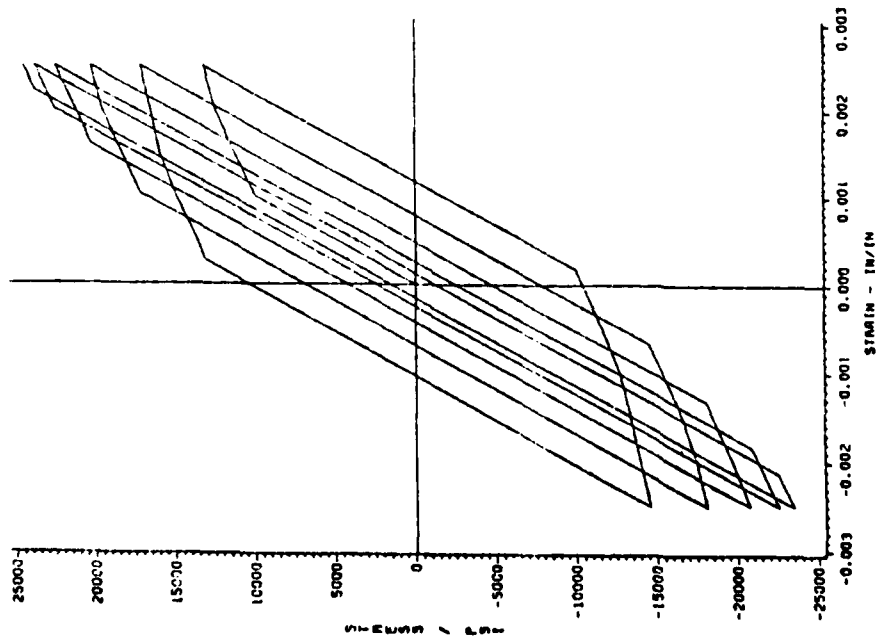


Isotropic Hardening

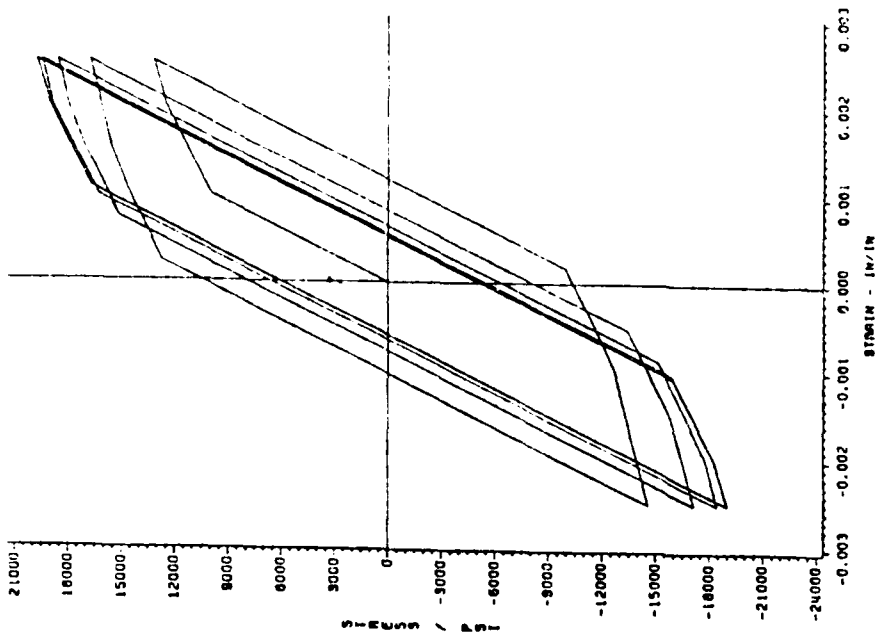


Kinematic Hardening

Fig. 12 Modeling of cyclic saturation using kinematic and isotropic hardening laws



Combined hardening with β constant



Combined hardening with a function of plastic strain

Fig. 13 Modeling of cyclic saturation using combined hardening law

Example 3 - Cyclic thermomechanical loading. This example is similar to one in reference [25] but is still applicable here to show the increased capabilities of the revised model in predicting the strain hardening behavior and also in reiterating its nonisothermal aspects. Depicted in Fig. 14 are the input stress-strain curves and thermomechanical load history for a hypothetical test. Note that these curves do not include the capacity for variable hardening in order to maintain clarity of the example. The hardening ratio is a constant one-half.

Results from the constitutive model are shown in Fig. 15 where t_i in this figure corresponds to t_i in Fig. 14. Modulus, strain hardening, and yield surface size changes with temperature are all shown.

It is also interesting to look at the resulting yield surface size vs. plastic strain diagram for this example also shown in Fig. 15. As discussed previously in construction of these diagrams, the curves are modified everytime there is a stress reversal which causes yield. This physically represents the rounded shape of the stress-strain curve after reverse yielding seen in experiment. In terms of modelling, this corresponds to "linking" the original K vs. $\bar{\epsilon}^p$ curves onto the current global diagram also explained in the section on construction of these diagrams. The squares in Fig. 15 point out where this process takes place each time. The curves at each temperature are modified for linear interpolation purposes.

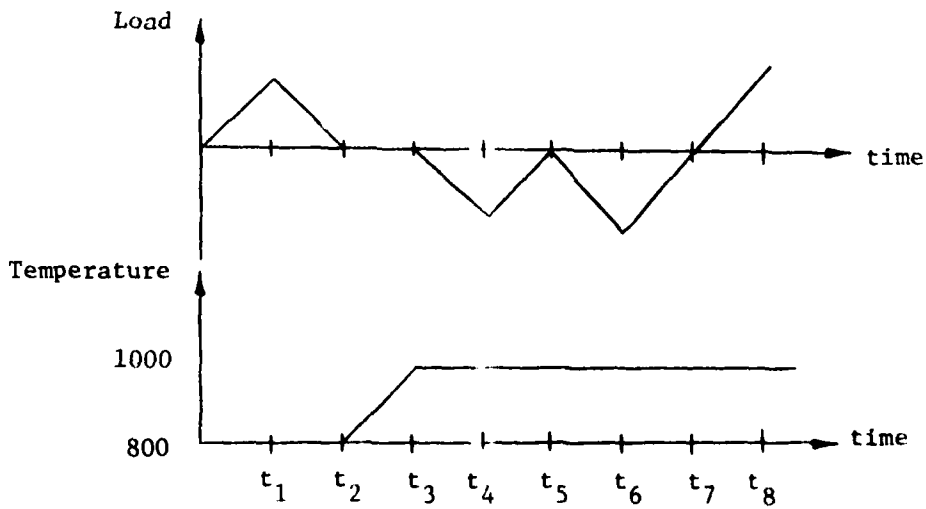
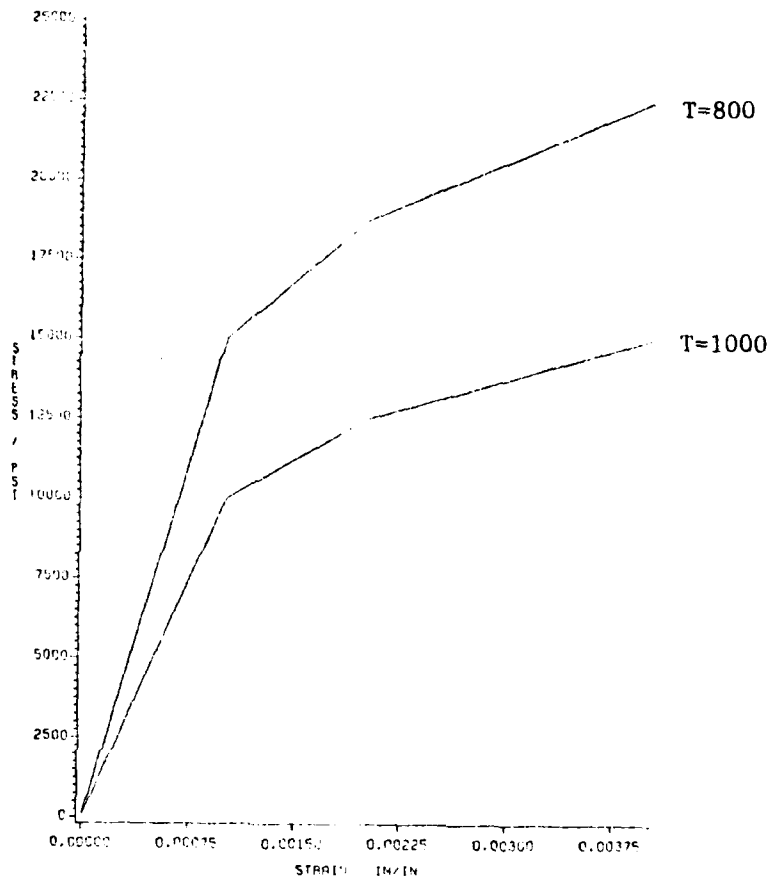


Fig. 14 Input for Example 3

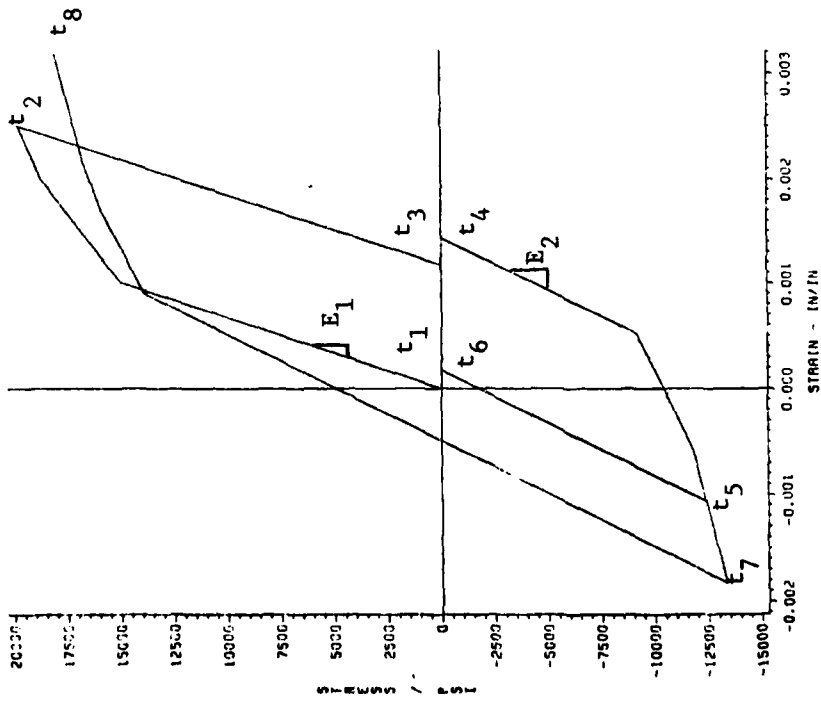
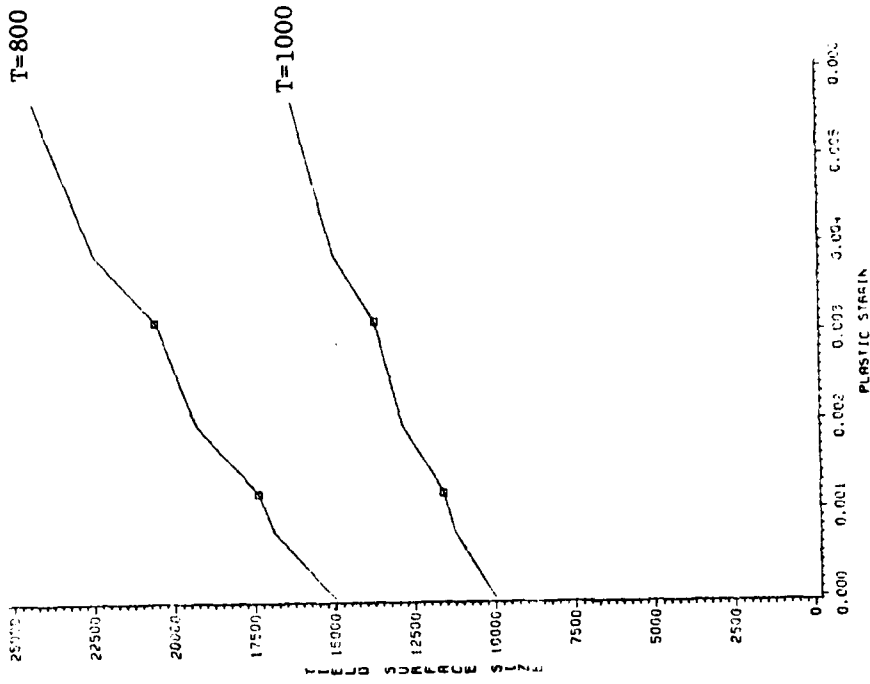


Fig. 15 Cyclic thermomechanical loading

Comparison with Experiment

As discussed earlier, characteristics of metals such as the high rate of strain hardening upon yield reversal are much more pronounced at high strain rates and temperatures below one-half the melting point. Modelling of this phenomenon is less critical at more elevated temperatures where plastic deformation is more fully rate controlled. More importantly, there is an intermediate temperature range where the coupling of plasticity and rate effects is the most critical test of the constitutive model. To evaluate the models capabilities in all of these environments, specific areas of testing are: (1) elevated temperature tests that evaluate the rate independent capabilities of the model, (2) cyclic load tests that evaluate the modelling of the Bauschinger effect, the change in strain hardening upon stress reversal, yield surface evolution, and cyclic saturation, (3) transient temperatures tests that evaluate the modelling of thermally dependent material properties, (4) high temperature tests that evaluate the rate dependent capabilities of the model, and (5) thermoelastic-plastic-creep tests that evaluate the capabilities in the intermediate temperature range.

The high temperature materials testing laboratory in the mechanical engineering department of Texas A&M University was used to run all tests. A Mechanical Testing Systems (MTS) machine along with an induction heating coils and generator, optical and thermocouple type temperature controllers, high temperature tension-compression grips, a high temperature diametral strain extensometer, and constant stress creep frames fully outfitted for high temperature testing are the main components available in this lab.

Cyclic thermomechanical load test on 5086 aluminum alloy. The first experimental evaluation is for a thermomechanical load history applied to a 5086 aluminum alloy. This test is very similar to Example 3. Fig. 16 shows the results of comparing the Allen and Haisler model using several different constant hardening ratios to experiment. One can observe both of the shortcomings of the model discussed earlier. The theoretical strain hardening behavior upon reyield is much too flat or square and the cyclic hardening predictions are inadequate. By inputting a second stress strain curve to characterize the more rounded strain hardening behavior and making the hardening ratio a function of plastic strain as in the revised model, this experiment can be modeled very well. The actual function of plastic strain used for β is that $\beta=0.45$ (constant) for the first quarter cycle and since the isotropic component of the yield surface saturated very quickly in the observed experimental results, the second quarter cycle was treated as being kinematic in nature. These results are shown in Fig. 17.

Cyclic loading of 304 stainless steel at 1000^oF. Several other model features are demonstrated by this test. As seen in Fig. 18, the compressive strain hardening behavior in the first cycle is more rounded in shape than the tensile behavior. It is believed that the same behavior would be seen on the first and second quarter cycles if compression preceded tension. Unlike the previous test on aluminum, this difference seems to alternate throughout all four cycles presented in Fig. 18. Thus one must alternate between first quarter and second quarter cycle input stress-strain data to model this test well.

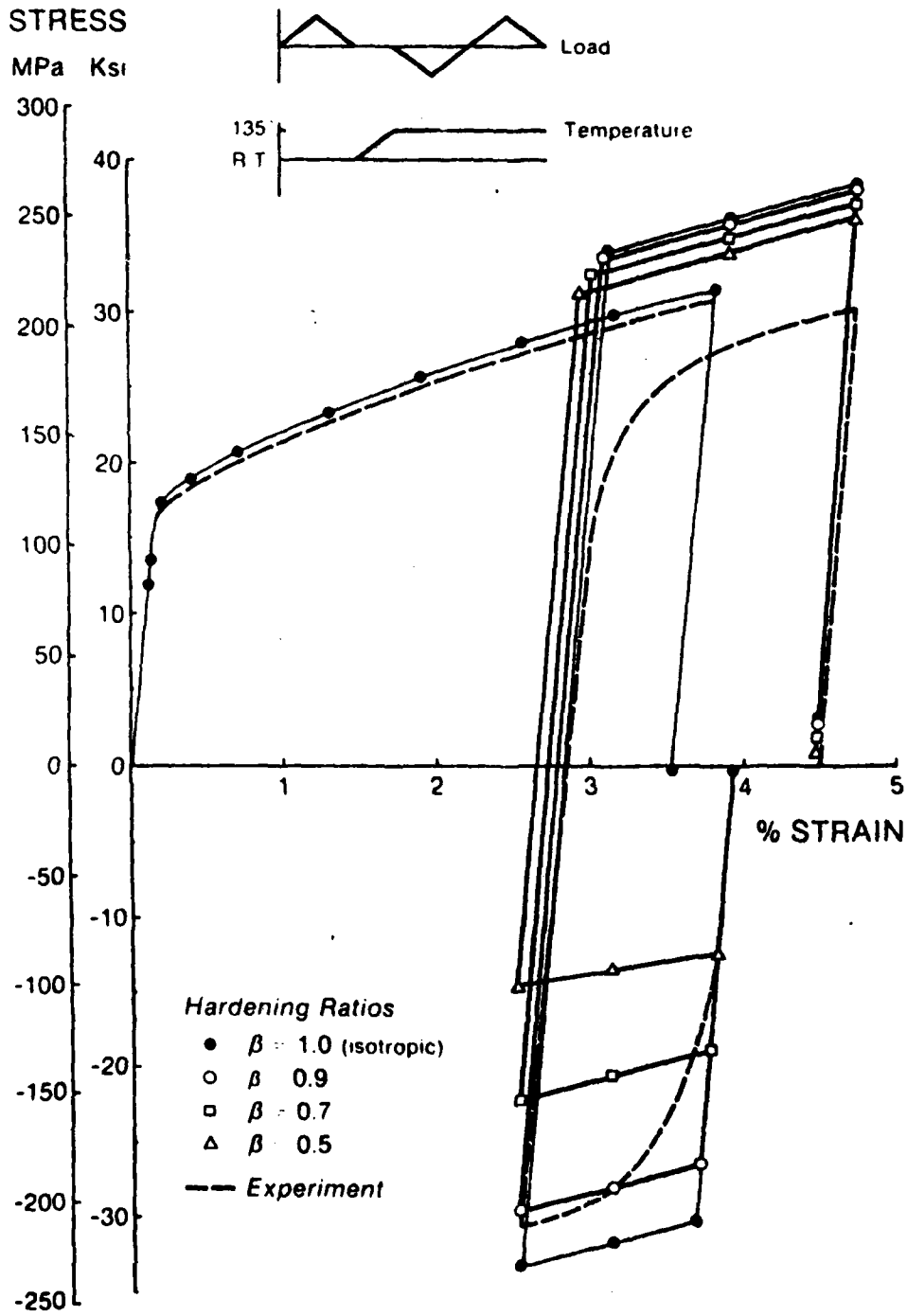


Fig. 16 Comparison of Allen and Haisler model to experiment for aluminum cyclic load test

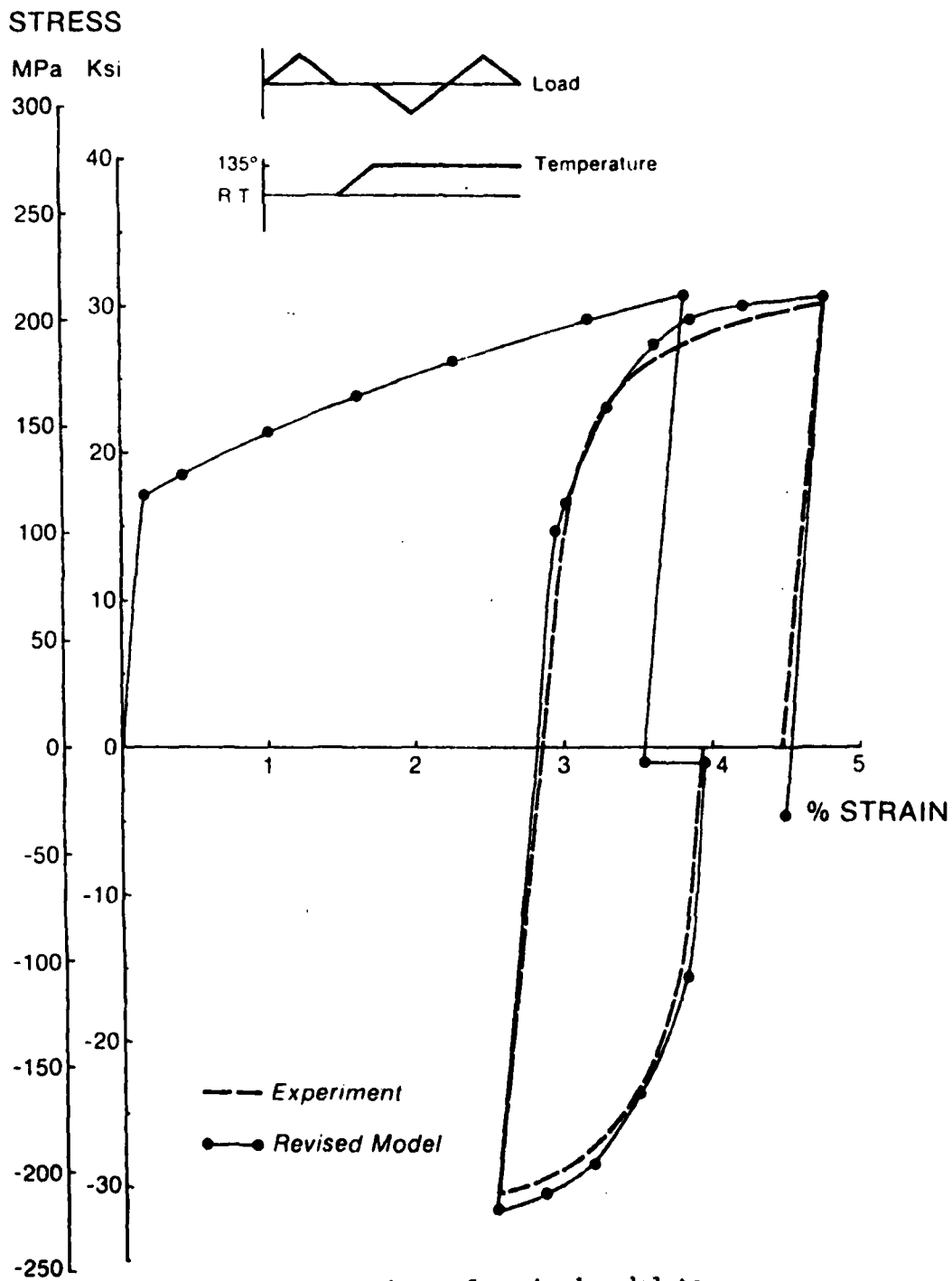


Fig. 17 Comparison of revised model to experiment for aluminum cyclic load test

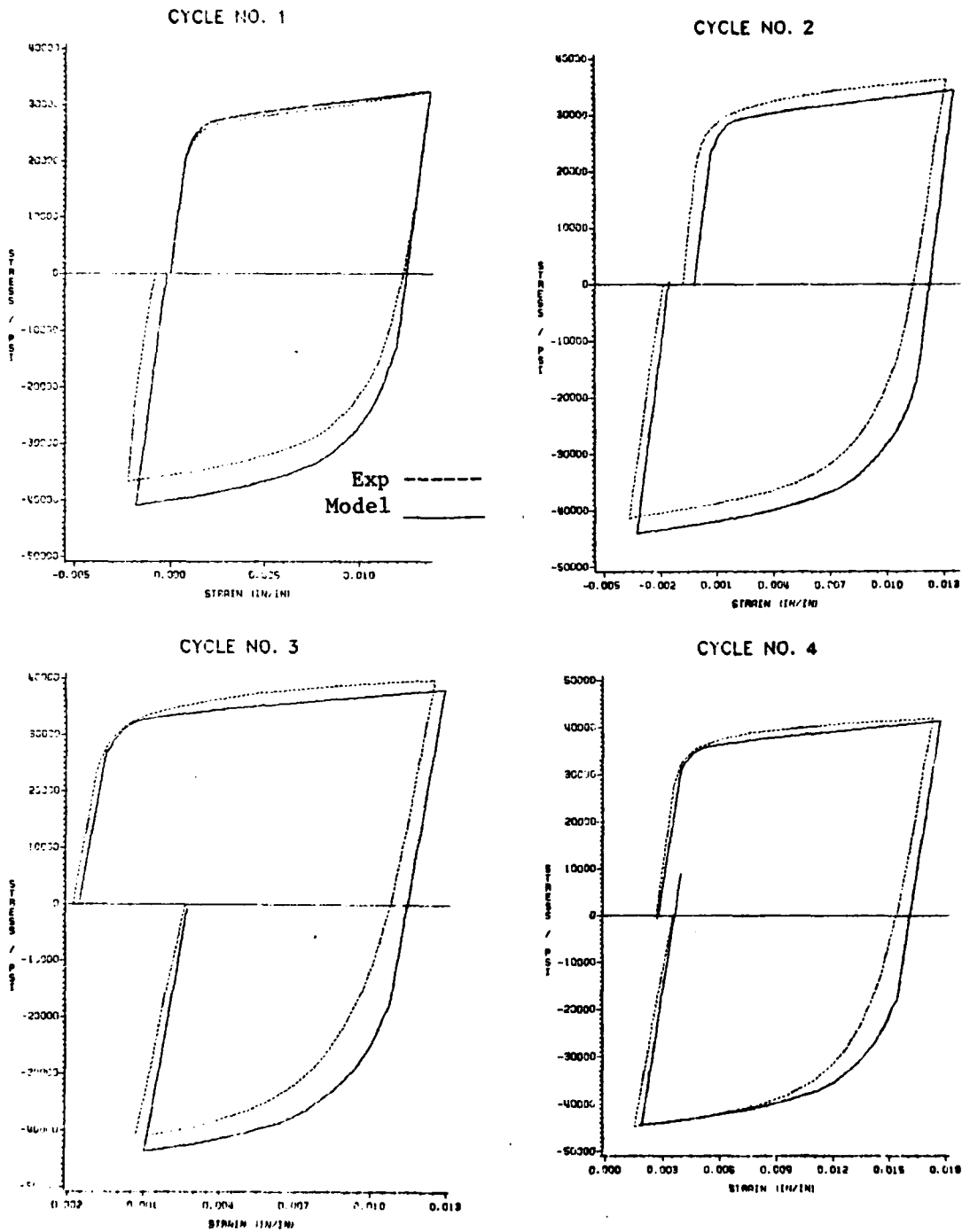


Fig. 18 Comparison of model and experiment for 304 stainless steel at 1000°F using first cycle data as input. A hardening ratio of 0.2 in tension and 0.35 in compression was used

One possible explanation for this alternating strain hardening behavior could be that the initial yield sets up an asymmetric microstructure. This phenomenon could also be explained by reasoning that there is less resistance to grain boundary sliding in tension as compared to compression. It is clear that a similar test needs to be performed with the initial yield in compression and then alternating tension and compression.

Next, the ability to vary the hardening ratio between alternating quarter cycles is demonstrated. In addition, Fig. 19 shows the results of using fourth cycle data as input. Both Fig. 18 and Fig. 19 show good correlation of the model with experiment. An interesting observation is that the elastic modulus during unloading decreases slightly in the experimental results. This is not taken into account by the constitutive model and is the reason for most of the discrepancy between experiment and model predictions.

Cyclic saturation of hastelloy-X. In Chapter 3, there was a discussion concerning cyclic saturation. Recall that cyclic saturation is the limiting periodic response in which the stress-strain curve for each consecutive cycle is the same as shown in Fig. 5 (p. 28). Although most materials show a gradual hardening during this saturation process, some materials may cyclically soften. Microphysically this corresponds to the movement of dislocations from a random orientation into a cell structure which stabilizes their movement. This results in the limiting response of the material. At more elevated temperatures, the saturation effect naturally becomes faster as the mobility of the dislocation increases with increasing temperature. Hastelloy-X

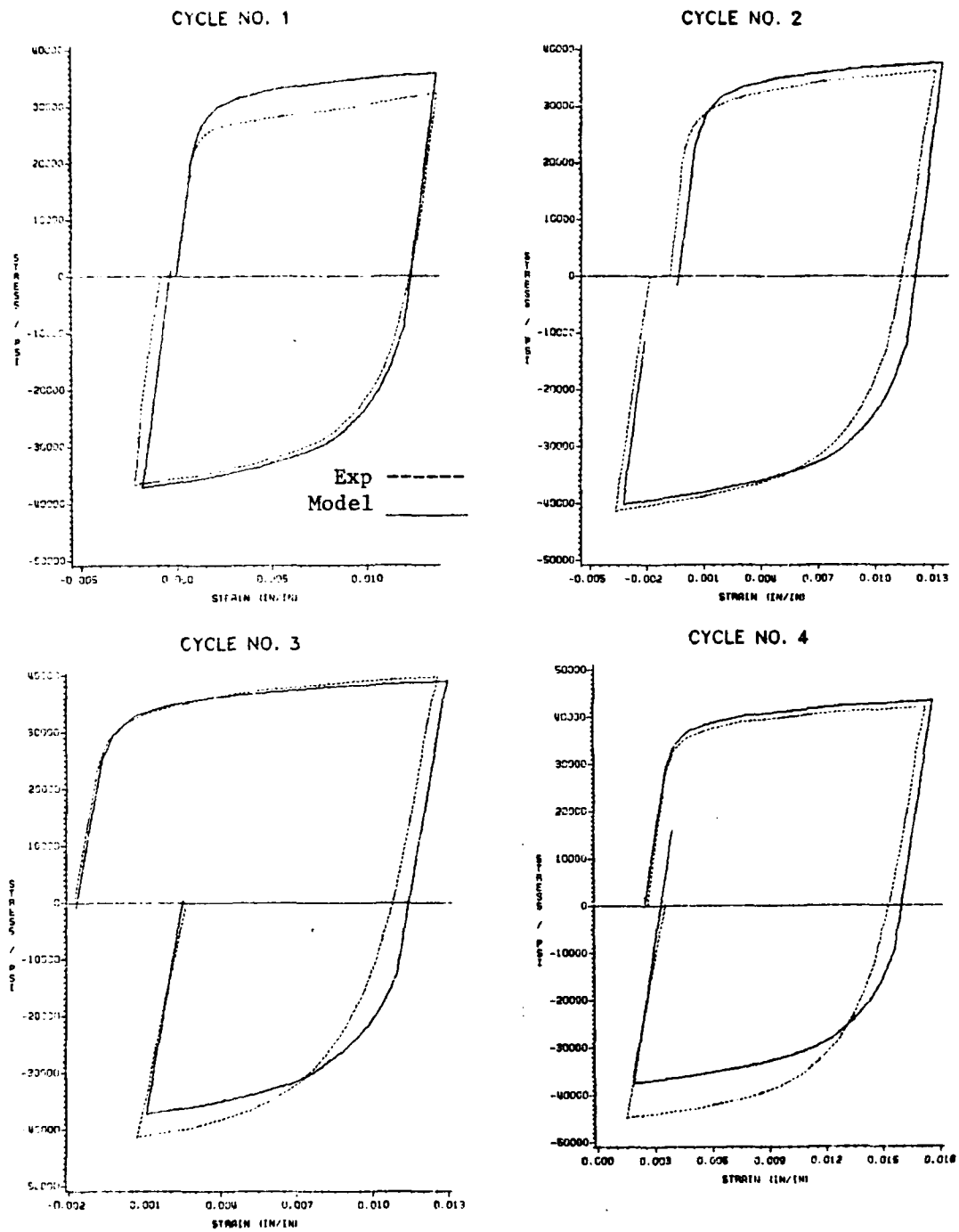


Fig. 19 Comparison of model and experiment for 304 stainless steel at 1000°F using fourth cycle data as input. A hardening ratio of 0.15 in tension and 0.28 in compression was used

displays cyclic saturation as shown in Figs. 20-25. These curves are actual experimental results of load vs. diameter change from the MTS machine. The abrupt drops in stress at various points are not due to machine problems but are rather due to dynamic strain aging of the material.

The center diagram in Fig. 20 shows the cyclic saturation discussed above. Uniaxial specimens were cycled under strain control (diametral strain) between equal tension and compression strain ranges until saturation occurred. In order to observe strain rate effects, most tests were run at three rates corresponding to test times of 10, 30, and 300 seconds per quarter cycle. During the test the diameter change rate was constant so that actual axial strain rate was variable during the cycle; however, the above test times correspond to average axial strain rates of 1.1×10^{-3} , 3.67×10^{-4} , and 3.67×10^{-5} in/in/sec. These rates were chosen because they are typical of strain rates seen under normal operating conditions of hot gas turbines. Notice that at room temperature, the rate dependent inelastic strain is negligible as the hysteresis loops do not change with different diameter change rates. Fig. 21 and Fig. 22 show the results for the same strain history at 500°F and 900°F, respectively. To define the rate dependent inelastic strain, a reference hysteresis loop is utilized as was outlined in Chapter 3. Comparing Figs. 22 and 23, it is seen that rate dependence of the saturated hysteresis loops is insignificant below 900°F for the rates considered. Consequently, the reference temperature is chosen as 900°F.

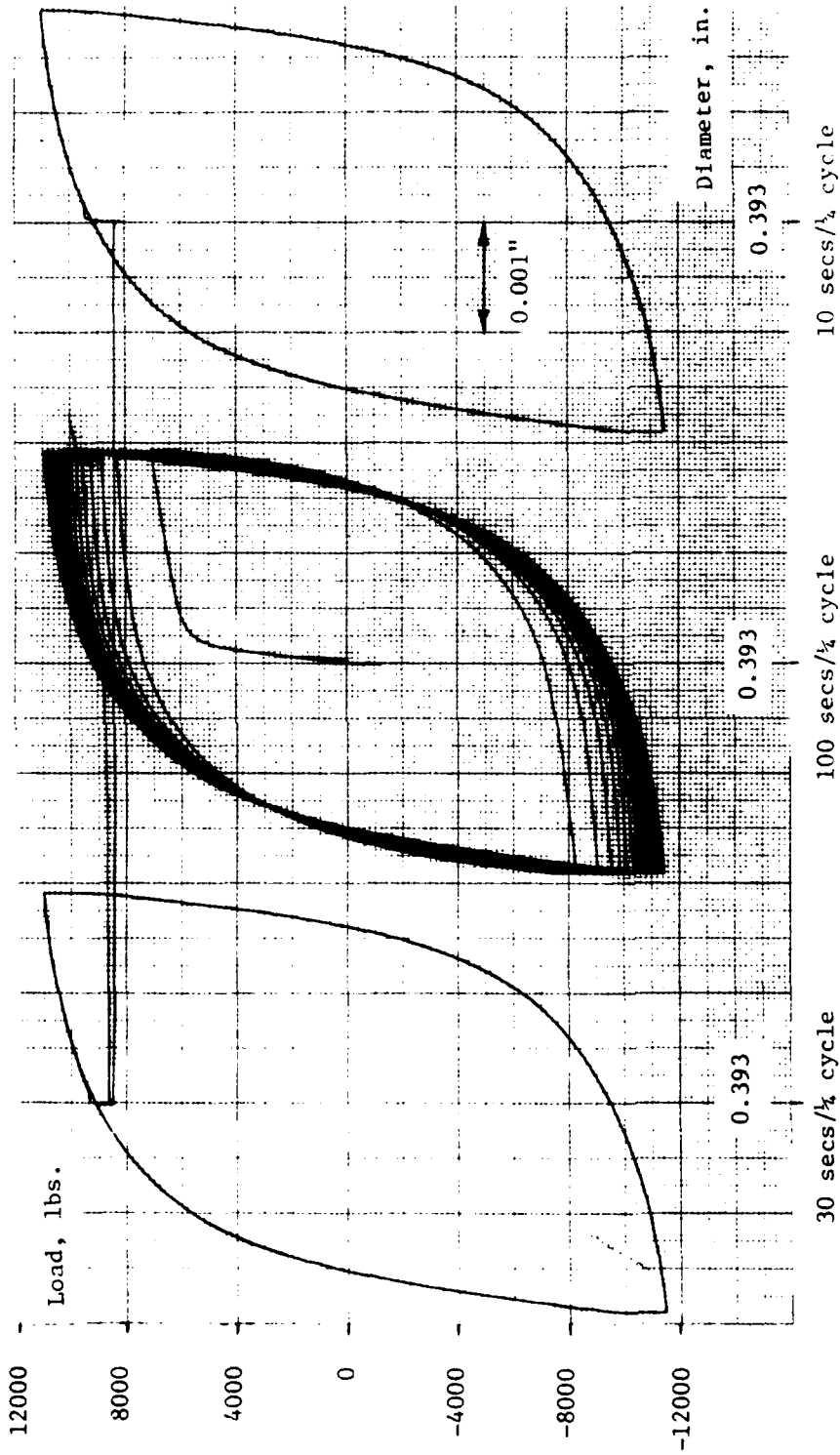


Fig. 20 Experimental hysteresis loops for hastelloy-X at room temperature

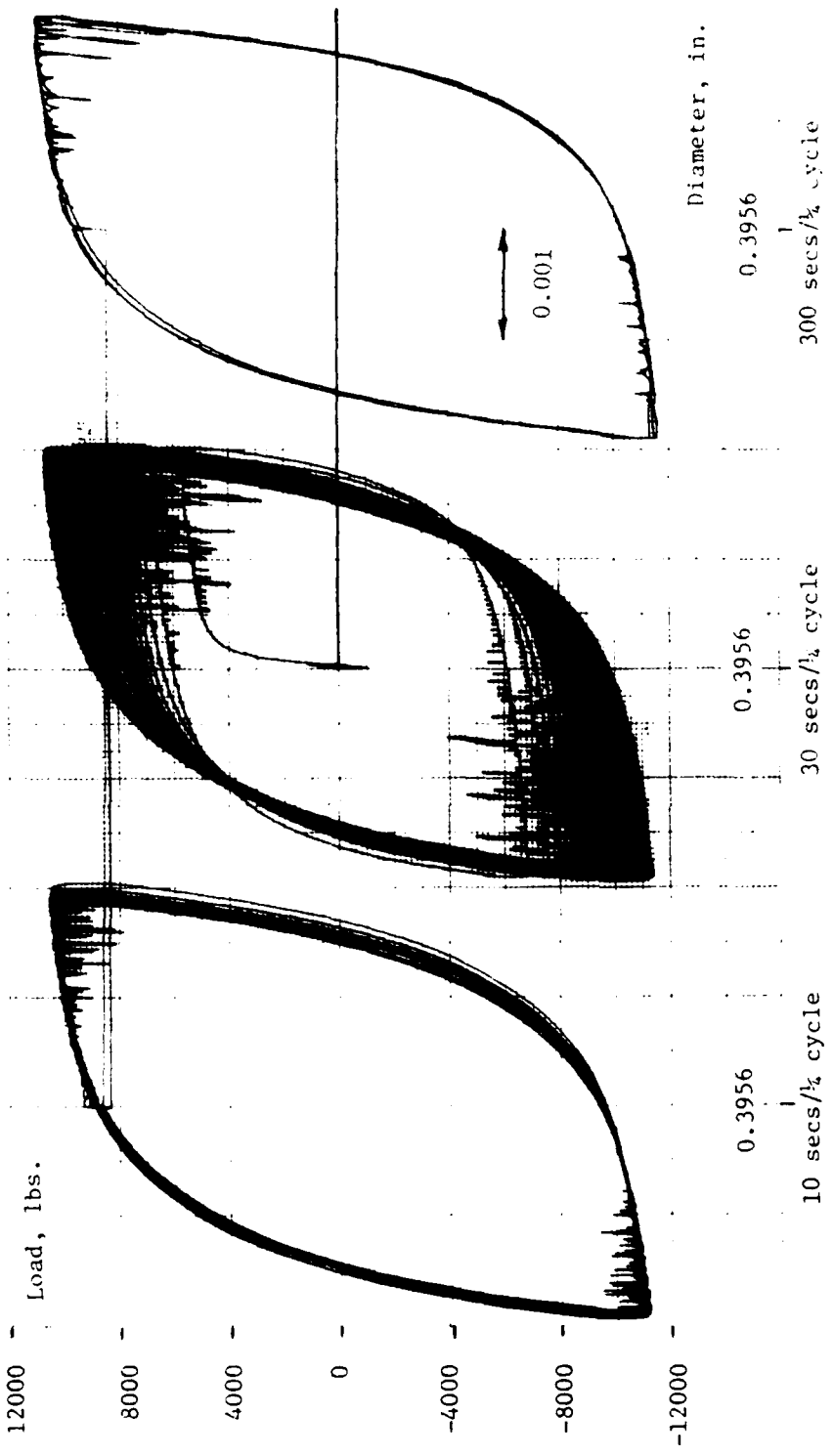


Fig. 21 Experimental hysteresis loops for hastelloy-X at 500°F

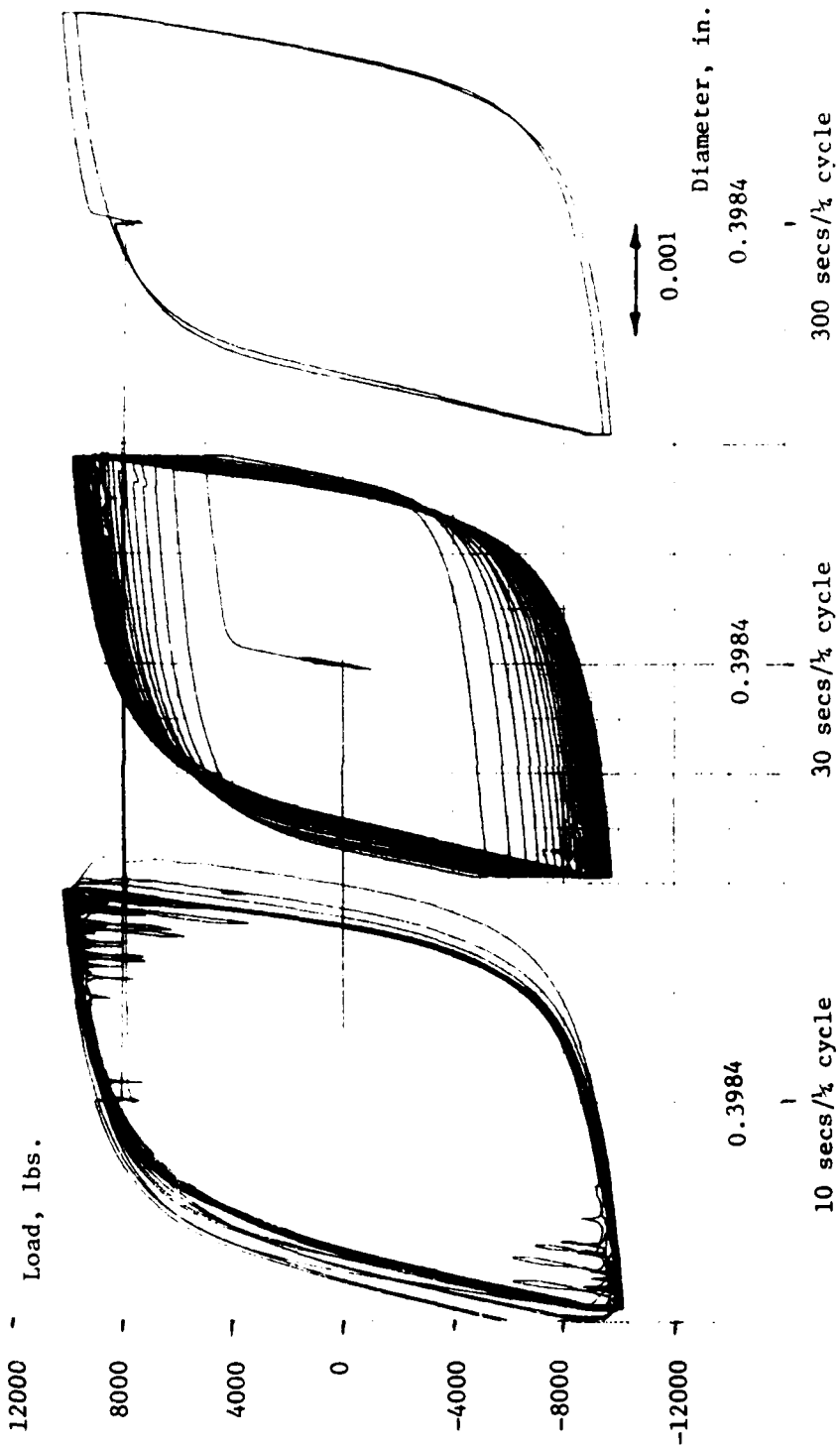


Fig. 22 Experimental hysteresis loops for hastelloy-X at 900°F

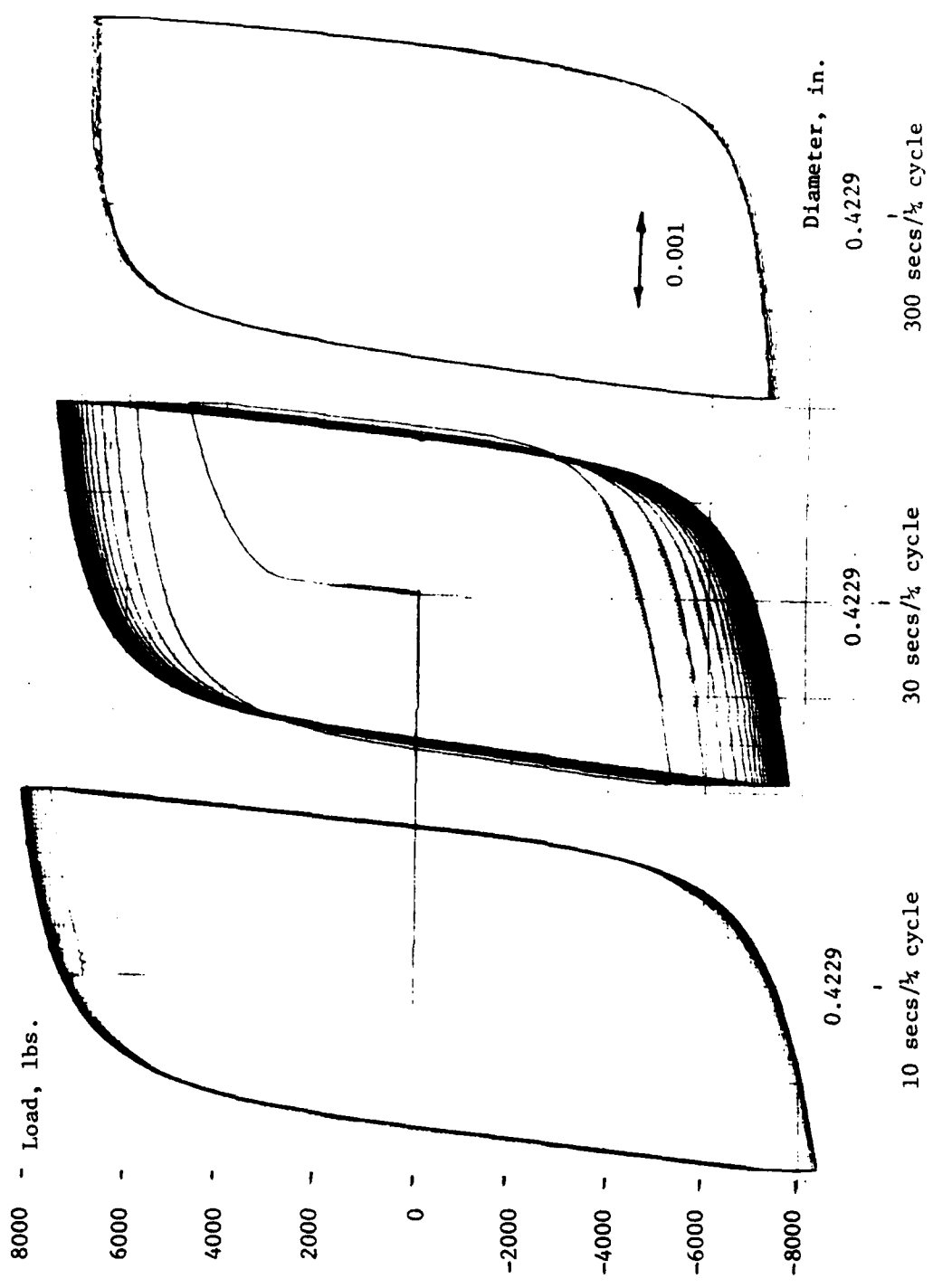


Fig. 23 Experimental hysteresis loops for hastelloy-X at 1200°F

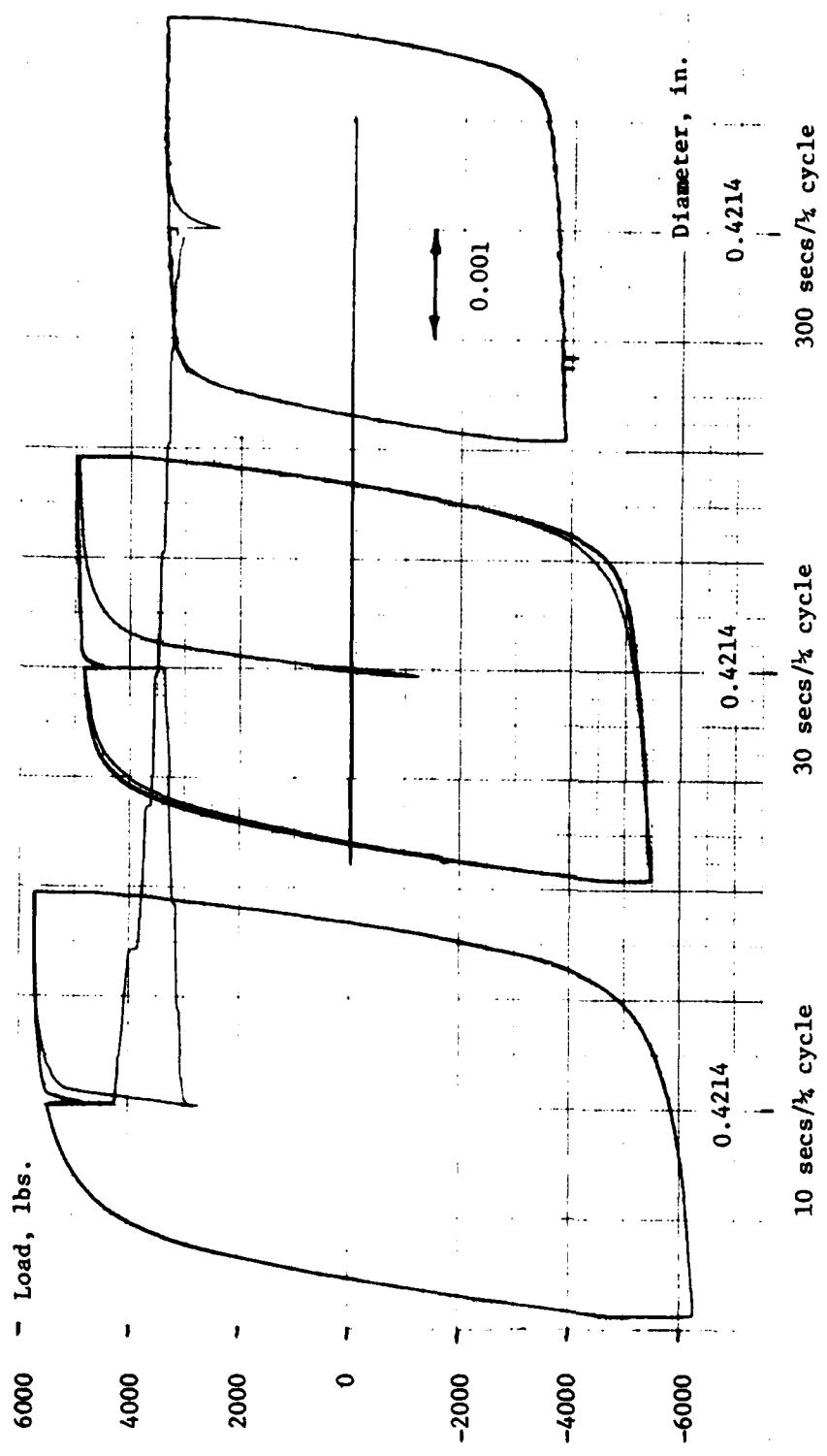


Fig. 24 Experimental hysteresis loops for hastelloy-X at 1400°F

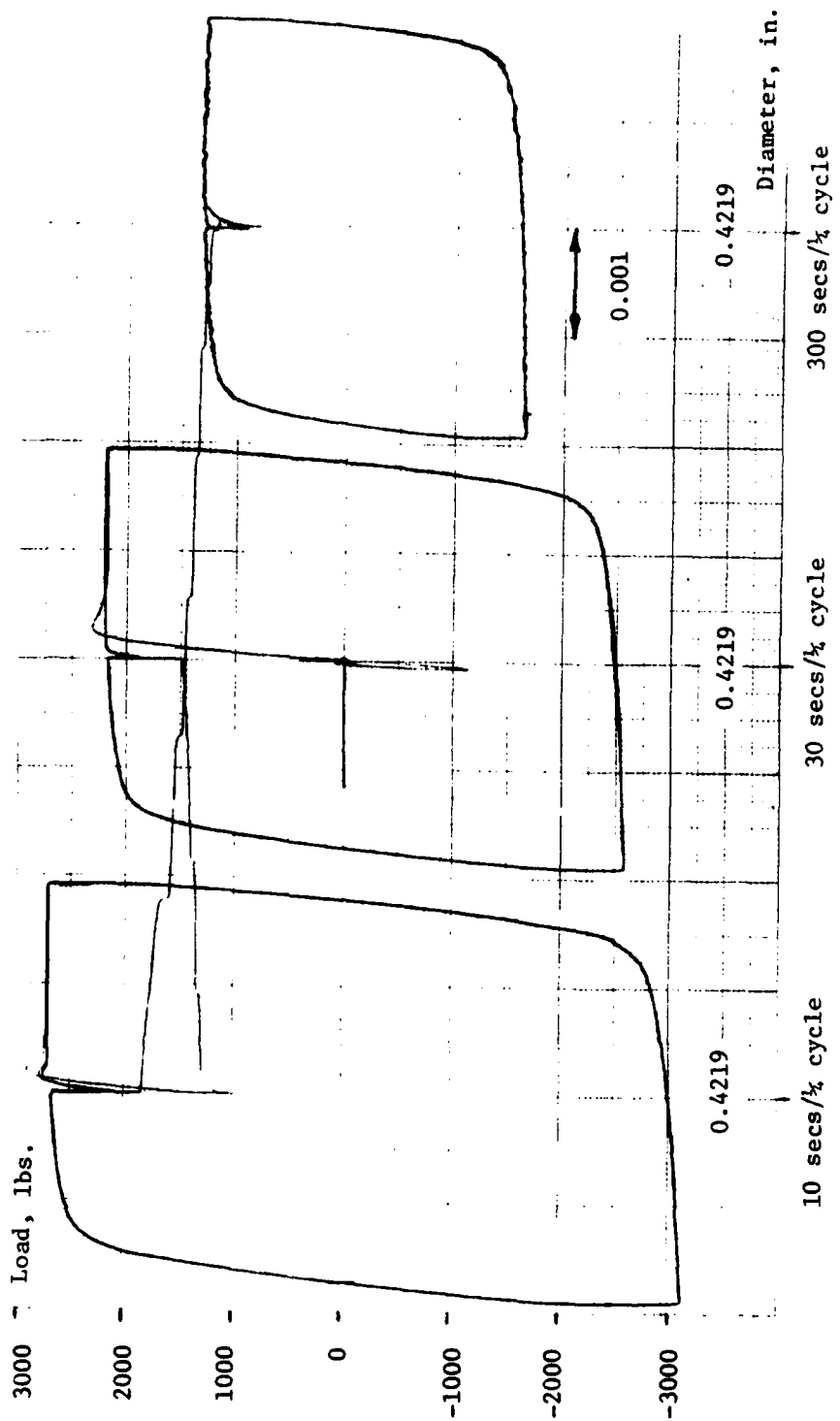


Fig. 25 Experimental hysteresis loops for hastelloy-X at 1600°F

An interesting phenomenon most clearly evident in Fig. 21 is the discontinuities or serrations seen in the curves. This is known as dynamic strain aging and is associated with interactions between moving dislocations and solute atoms [37]. Dynamic strain aging is both temperature and strain rate dependent.

At 1200°F, the rate dependent inelastic strain is no longer negligible. Fig. 23 shows the somewhat faster saturation and more "square" shape of the hysteresis loops. These effects are even more pronounced at 1400°F and 1600°F as depicted in Fig. 24 and Fig. 25. At these elevated temperatures the rate dependence dominates and can be modelled very well with an equation like equation (35). The hysteresis loops are quite square in nature, and a high rate of strain hardening upon stress reversal is not seen. A critical test of a constitutive theory would be in modelling the behavior in Fig. 23 where both rate independent plasticity and rate dependent creep are important.

Theoretical modelling of cyclic saturation of hastelloy-X was performed for the room temperature case. The results are shown in Fig. 26. Experimental stress-strain data is shown only for the first one-half cycle and the last (saturated) cycle. The model results depict the gradual saturation response as well as the limiting response. A hardening ratio of $\beta = -0.375\bar{\epsilon}^P + 0.075$ was used in tension and $\beta = -0.5\bar{\epsilon}^P + 0.10$ was used in compression. Notice that when the model predictions approach saturation, some fluctuation is seen on the compression side. This is thought to be due to increasing numerical error at this point as no equilibrium iterations are performed. Most

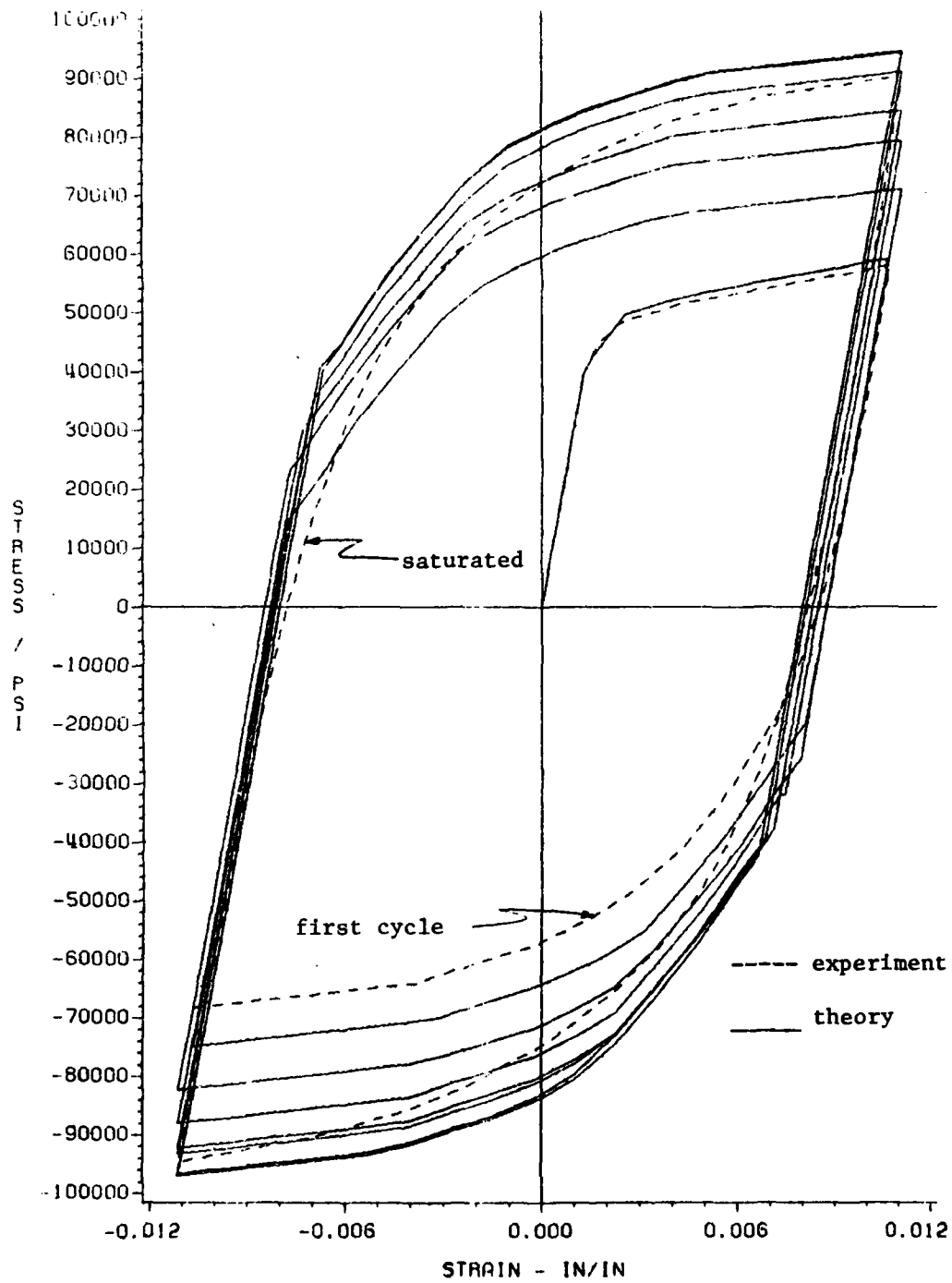


Fig. 26 Cyclic saturation of hastelloy-X at room temperature

of the difference in experiment and theory is due to difficulty in modeling of the second quarter cycle, otherwise the model predictions are quite good.

CHAPTER V

CONCLUSIONS

An uncoupled, incremental constitutive model for elastic-plastic behavior of metals at elevated temperatures has been presented. Revisions to the combined kinematic-isotropic hardening rule allow for much improved modelling of cyclic phenomenon. Also, an alternative approach to characterizing the rate dependent inelastic deformation has been proposed.

Successful evaluation of the constitutive model against experiment has been accomplished for a limited range of tests. The Bauschinger effect, change in strain hardening upon stress reversal, yield surface evolution, and cyclic saturation are all modeled well for the isothermal, rate independent case at elevated temperature. Unfortunately, no comparison of the theory to experiment have been performed at this time for the load and temperature ranges where rate dependence is a significant factor. The need to utilize an improved model like that presented herein depends on the application. For example, if the application is to life or fatigue predictions, then the detailed modelling of saturation and strain hardening observed at low temperatures may not be of utmost importance. The saturated hysteresis loop may be adequate to define long term fatigue response. Conversely, for low cycle applications, many researchers in this field are concerned with exact hysteresis loop predictions and the evolution to saturation. In this case, the improved model has important

applications. Finally, in regards to the rate dependence of the model, experimental results seem to indicate that the uncoupling presented in Chapter 3 gives acceptable predictions, but further tests are needed to verify the model.

REFERENCES

1. Tresca, H., "Notes on Yield of Solid Bodies Under Strong Pressure," Comptes Rendus del' Academie des Sciences, Vol. 59, 1864, p. 754.
2. Hill, R., The Mathematical Theory of Plasticity, Oxford University Press, London, 1950.
3. von Mises, R., "Mechanik der Fescen Koerper in Plastisch Deformablen Zustant," Goettinger Nachr., Math-Phys. Kl., 1913, pp. 582-92.
4. Prandtl, L., "Spannungsverteilurg in Plastischen Koerper," Proceedings of the First International Congress on Applied Mechanics, Delft, Technische Boekhandel en Druckerij, Jr. Waltman, Jr., 1925, pp. 43-45.
5. Reuss, E., "Bereuchsichtigung der Elastischen Formaenderungen in der Plastizitaetstherie," Zeitschrift fuer Angewandte Mathematic und Mechanik, Vol. 10, 1930, pp. 266-274.
6. Drucker, D. C., "A Definition of Stable Inelastic Material," Journal of Applied Mechanics, Vol. XVII, 1959, pp. 55-65.
7. Prager, W., "The Theory of Plasticity: A Survey of Recent Achievements," Proceedings of the Institution of Mechanical Engineers, London, Vol. 169, 1955, pp. 41-57.
8. Ziegler, H., "A Modification of Prager's Hardening Rule," Quarterly of Applied Mechanics, Vol. XVII, 1959, pp. 55-65.
9. Walker, K. P., "Representation of Hastelloy-X Behavior at Elevated Temperature with a Functional Theory of Viscoplasticity," presented at ASME Pressure Vessels Conference, San Francisco, August 12, 1980.
10. Allen, David H., and Milly, Teresa M., "A Comparison of Constitutive Models for Nonlinear Rate Dependent Material Behavior of Solids," Virginia Polytechnic Institute and State University Report No. VPI-E-80.16, Blacksburg, Virginia, Sept. 1981.
11. Krieg, R. D., Swearingen, J. C., and Rohde, R. W., "A Physically-Based Internal Variable Model for Rate-Dependent Plasticity," Proceedings ASME/CSME PVP Conference, 1978, pp. 15-27.
12. Allen, David H., "A Model for Predicting Response of Nonlinear Materials Subjected to Thermomechanical Loading," Dissertation, Texas A&M University, Aug. 1980.
13. Hunsaker, B. Jr., "An Evaluation of Four Hardening Rules of the Incremental Theory of Plasticity," Tnesis, Texas A&M University Dec. 1973.

14. Polakowski, N. H., and Ripling, E. J., Strength and Structure of Engineering Materials, Prentice-Hall, Inc., Englewood Cliffs, N.J., 1966.
15. Bodner, S. R., Partom, I., and Partom, Y., "Uniaxial Cyclic Loading of Elastic-Viscoplastic Materials," Journal of Applied Mechanics, Vol. 46, December 1979, pp. 805-810.
16. Miller, A. K., "Modelling of Cyclic Plasticity with Unified Constitutive Equations: Improvements in Simulating Normal and Anomalous Bauschinger Effects," Journal of Engineering Materials and Technology, Vol. 102, April 1980, pp. 215-222.
17. Kocks, U. F., "Laws for Work-Hardening and Low-Temperature Creep," Journal of Engineering Materials and Technology, Vol. 98, January 1976, pp. 76-85.
18. Walker, K. P., "Research and Development Program for Nonlinear Structural Modelling with Advanced Time - Temperature Dependent Constitutive Relationships," First Quarterly Technical Narrative, Pratt & Whitney Aircraft Group Report No. PWA-5700-6, January 1980.
19. Allen, David H., "Course Notes for MM641 - Plasticity Theory," Texas A&M University, unpublished, Summer 1980.
20. Petersson, Hans, and Popov, Egor P., "Constitutive Relations for Generalized Loadings," Journal of the Engineering Mechanics Division, ASCE, Vol. 103, No. EM4, Aug. 1977, pp. 611-27.
21. Popov, Egor P., and Petersson, Hans, "Cyclic Metal Plasticity: Experiment and Theory," Journal of the Engineering Mechanics Division, ASCE, Vol. 104, Dec. 1978, pp. 1371-87.
22. Snyder, M. D., and Bathe, K. J., "Formulation and Numerical Solution of Thermo-Elastic-Plastic and Creep Problems," National Technical Information Service, No. 82448-3, June 1977.
23. Yamada, Y., "Constitutive Modelling of Inelastic Behavior of Numerical Solution of Nonlinear Problems by the Finite Element Method," Computers and Structures, Vol. 8, 1978, pp. 533-43.
24. Yamada, Y., and Sakurai, T., "Basic Formulation and a Computer Program for Large Deformation Analysis," Pressure Vessel Technology, Part I, ASME, 1977, pp. 341-52.
25. Allen, David H., and Haisler, Walter W., "A Theory for Analysis of Thermoplastic Materials." Computers and Structures, Vol. 13, 1981, pp. 124-35.
26. Zienkiewicz, O. C., The Finite Element Method, McGraw-Hill, London, 1977.

27. Fung, Y. C., Foundations of Solid Mechanics, Prentice-Hall, Inc., Englewood Cliffs, N.J., 1965.
28. Hunsaker, B. Jr., "The Application of Combined Kinematic-Isotropic Hardening and the Mechanical Sublayer Model to Small Strain Inelastic Structural Analysis by the Finite Element Method," Dissertation, Texas A&M University, August 1976.
29. Allen, David H., "A Note on the Combined Isotropic-Kinematic Work Hardening Rule," International Journal for Numerical Methods in Engineering, Vol. 15, 1980, pp. 1724-28.
30. Pugh, C. W., Corum, J. M., Lin, K. C., and Greenstreet, W. L., "Currently Recommended Constitutive Equations for Inelastic Design Analysis of FFTF Components," ORNL TM-3602, Oak Ridge National Laboratory, Oak Ridge, Tenn., Sept. 1972.
31. Dafalias, Y. F., and Popov, E. P., "Plastic Internal Variables Formalism of Cyclic Plasticity," Journal of Applied Mechanics, Vol. 43, Dec. 1976, pp. 645-51.
32. Caulk, D. A., and Naghdi, P. M., "On the Hardening Response in Small Deformation of Metals," Journal of Applied Mechanics, Vol. 45, December 1978, pp. 755-64.
33. Swindeman, R. W., and Pugh, C. E., "Creep Studies on Type 304 Stainless Steel (Heat 8043813) Under Constant and Varying Loads," ORNL-TM-4427, June 1974, Oak Ridge National Laboratory, Oak Ridge, Tenn.
34. Haisler, W., "Application of an Uncoupled Elastic-Plastic Creep Constitutive Model to Metals at High Temperatures," to be presented at the Symposium on Nonlinear Constitutive Relations for High Temperature Applications, The University of Akron, Akron, Ohio, May 19 and 20, 1982.
35. Bradley, W. L., "A New Uncoupled, Viscoplastic Constitutive Model," to be presented at the Symposium on Nonlinear Constitutive Relations for High Temperature Applications, The University of Akron, Akron, Ohio, May 19 and 20, 1982.
36. Allen, David H., "Computational Aspects of the Nonisothermal Classical Plasticity Theory," Virginia Polytechnic Institute and State University Report No. VPI-E-80.29, Blacksburg, Virginia, Oct, 1980.
37. Reed-Hill, Robert E., Physical Metallurgy Principles, D. van Nostrand Company, New York, 1964.

APPENDIX

COMPUTER PROGRAM OUTLINE

The following outline describes a basic flowchart of the uniaxial constitutive equations for a given total strain increment. Subincrementation (forward integration) with no equilibrium iterations is the solution technique used. Note that in the setup of any problem, the yield surface size and equivalent uniaxial stress vs. plastic strain diagrams are initialized using the first set of input stress-strain curves.

- A. Set up subincrementation on strain, temperature, and time increments.
- B. Compute elastic modulus and the change in the elastic modulus due to temperature increment. Linearly interpolate between input values if necessary.
- C. Compute thermal strain increment. Linear interpolation may be necessary to obtain thermal expansion coefficient. [equation (51)]
- D. Compute creep strain increment based on stress at beginning of step and temperature at end of step. [CHAPTER III - Creep strain increment]
- E. Compute trial stress increment assuming elastic behavior. Add this to the stress at beginning of step to obtain total stress.
- F. Check for yielding
 1. Compute yield function. [equation (34)]
 2. Compute yield surface size for current value of equivalent

- uniaxial plastic strain at temperatures at start and end of load step.
3. Compare yield function value with current yield surface size.
 - a. If elastic, go to step N'.
 - b. If yielded and last step was elastic-plastic go to step J.
 - c. If yielded and last step was elastic, go to step G.
 - G. Update stress and strain to yielded portion for transition step. [equations (46) and (47)]
 1. Subtract assumed elastic stress increment from total since this step is elastic-plastic.
 2. Compute ζ and η factors. [equations (48) and (50)]
 3. Update total strain, elastic strain, and creep strain to yield surface.
 - H. Compute creep strain increment based on yield stress and temperature at end of step.
 - I. Modify global K and $\bar{\sigma}$ vs. $\bar{\epsilon}^P$ diagrams. [CHAPTER III - Construction of K and $\bar{\sigma}$ vs. $\bar{\epsilon}^P$ diagrams]
 1. If the hardening ratio is a function of plastic strain, recompute the base K and $\bar{\sigma}$ vs. $\bar{\epsilon}^P$ diagrams. [equations (39) - (41)]
 2. If this is the initial yield or yield has occurred without a stress reversal, no modification is necessary. Go to step J.
 3. If reverse yielding has occurred, modify the global diagrams. The particular material of interest determines whether the first or second base curves are used.

J. Experiencing elastic-plastic behavior.

1. Compute $\partial F/\partial \sigma$ and the gradients H' , $\partial \sigma/\partial T$, $\partial K/\partial \bar{\epsilon}^P$, $\partial K/\partial T$ for the current value of plastic strain and temperature.
[equations (42) - (45)]

K. Compute stress increment. [equation (29)]

In transition step from elastic to elastic-plastic behavior, only the leading term of equation (16) is used.

L. Compute strains and update totals.

1. Elastic strain. [equation (51)]
2. Plastic strain increment is the total minus the elastic, thermal, and creep increments.
3. Equivalent uniaxial plastic strain is the absolute value of the plastic strain increment for the uniaxial case.

M. Update yield surface center. In transition step the yield surface translation scalar is calculated assuming isothermal behavior for temperature at end of step.

1. Compute translation scalar. [equation (32)]
2. Compute change in yield surface center. [equation (6)]
3. Update yield surface center.

N. Update values to end of subincrement.

1. Stress.
2. Total strain.
3. Creep strain.
4. Thermal strain.

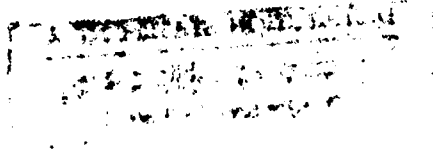
N'. Update values to end of load step for elastic case.

1. Stress.

2. Total strain.
 3. Elastic strain.
 4. Creep strain.
 5. Thermal strain.
0. Repeat above procedure for each subincrement.

REPORT DOCUMENTATION PAGE		READ INSTRUCTIONS BEFORE COMPLETING FORM
1. REPORT NUMBER 3275-82-1	2. GOVT ACCESSION NO. AD-A123035	3. RECIPIENT'S CATALOG NUMBER
4. TITLE (and Subtitle) Development and Evaluation of an Uncoupled, Incremental Constitutive Model for Elastic- Plastic-Creep Behavior at Elevated Temperatures		5. TYPE OF REPORT & PERIOD COVERED Final
		6. PERFORMING ORG. REPORT NUMBER
7. AUTHOR(s) Jeff Cronenworth and Walter E. Haisler		8. CONTRACT OR GRANT NUMBER(s) N00014-76-C-0150
9. PERFORMING ORGANIZATION NAME AND ADDRESS Department of Aerospace Engineering Texas A&M University College Station, TX 77843		10. PROGRAM ELEMENT, PROJECT, TASK AREA & WORK UNIT NUMBERS NR 064-534
11. CONTROLLING OFFICE NAME AND ADDRESS Office of Naval Research Department of the Navy Arlington, Virginia 22217		12. REPORT DATE May 1982
		13. NUMBER OF PAGES 86
14. MONITORING AGENCY NAME & ADDRESS (if different from Controlling Office)		15. SECURITY CLASS. (of this report)
		15a. DECLASSIFICATION/DOWNGRADING SCHEDULE
16. DISTRIBUTION STATEMENT (of this Report)		
<div style="border: 1px solid black; padding: 5px; display: inline-block;"> <p>DISTRIBUTION STATEMENT A Approved for public release Distribution Unlimited</p> </div>		
17. DISTRIBUTION STATEMENT (of the abstract)		
18. SUPPLEMENTARY NOTES		
19. KEY WORDS (Continue on reverse side if necessary and identify by block number)		
Plasticity Creep High Temperature Metals Constitutive Modelling		
20. ABSTRACT (Continue on reverse side if necessary and identify by block number)		
<p>A uniaxial, uncoupled constitutive model for predicting the response of thermal and rate dependent elastic-plastic material behavior is presented. The model is based on an incremental classical plasticity theory extended to account for thermal, creep, and transient temperature conditions. Revisions to the combined hardening rule of the theory allow for better representation of cyclic phenomenon including the high rate of strain hardening upon cyclic reyield and cyclic saturation. Also, an alternative approach is taken to</p>		

model the rate dependent inelastic deformation which involves hysteresis loops and stress relaxation tests at various temperatures. Evaluation of the model is performed by comparison with experiments involving various thermal and mechanical load histories on 5086 aluminum alloy, 304 stainless steel and Hastelloy-X.



LMED

-83